



Manuela Michlmayr, BSc.

Traumatic rupture of the aorta in traffic accidents

MASTER THESIS

to achieve the university degree of

Master of Science in Engineering
Master's degree program: Biomedical Engineering

submitted to

Graz University of Technology

Supervisor: Gerhard A. Holzapfel, Univ.-Prof. Dipl.-Ing. Dr.techn.
Institute of Biomechanics

Co-Supervisor: Florian Feist, Dipl.-Ing. Dr.techn.
Vehicle Safety Institute

Graz, May 2017

AFFIDAVIT

I declare that I have authored this thesis independently, that I have not used other than the declared sources/resources, and that I have explicitly indicated all material which has been quoted either literally or by content from the sources used. The text document uploaded to TUGRAZonline is identical to the present master thesis.

Date

Signature

Acknowledgment

My sincere gratitude goes to my co-supervisor Dipl.-Ing. Dr.techn. Florian Feist as well as Dipl.-Ing. Corina Klug who helped me in so many ways with the successful completion of this master thesis. I could count on their support, guidance and knowledge throughout the whole time of writing this master thesis.

I would like to express my deep gratitude to the head of the Institute of Biomechanics and my supervisor Univ.-Prof. Dipl.-Ing. Dr.techn. Gerhard A. Holzapfel for his support and the opportunity to carry out this master thesis. I would like to acknowledge Dipl.-Ing. Dr.techn. Gerhard Sommer for helping me with his expertise and knowledge.

I also want to express my gratitude to the head of Vehicle Safety Institute Univ.-Prof. Dipl.-Ing. Dr.techn. Hermann Steffan and Dipl.-Ing. Dr.techn. Wolfgang Sinz who gave me the opportunity to carry out this master thesis in cooperation with the Institute of Biomechanics.

I especially want to acknowledge my boyfriend Daniel and our daughter Julia for all their love, patience and support in finishing this work. They always believed in me and encouraged me in rough times.

Finally I would like to thank my parents and my boyfriend's mother for their constant support during my whole studies as well as my friends and colleagues for helping me anytime I needed an advice.

Abstract

In 2009 three children due to traumatic rupture of the aorta (TRA) suffered in a full-frontal vehicle impact. The accident can be considered as survivable in terms of the estimated velocity change Δv and the children were seated in child restraint systems complying with legal regulations. Back then, the accident was reconstructed by means of state-of-the-art multi body models. Contemporary finite element human body models (HBM), for application in impact biomechanics, allow a more detailed analysis of mechanisms leading to TRA, but the aorta model is very simplified in these models.

The objectives of this master thesis are to collect data about the relevance of TRA in traffic accidents in Austria, to summarize theories about injury mechanisms, to determine the most common location of TRA, to reconstruct the accident with HBMs, to establish an improved model of the vessel wall and to compare the behavior of this advanced model with a conventional aorta model used in HBMs.

TRA-cases of the accident database CEDATU (Central database for in-depth accident study) were analyzed in terms of location of rupture, age, gender, position in vehicle, type of accident and injury severity.

The aorta model of the HBMs was enhanced. A hyperelastic anisotropic material model with dispersion was selected in the explicit FEM solver LS-Dyna to model the three layers of the aorta (intima, media and adventitia). The material parameters were fitted to data from literature of uni-axial tests employing the optimization software Hyperstudy. The cylindrical segment of the aorta was qualitatively compared with and validated against experimental inflation tests. Next an impact-test was performed, where a cylindrical impactor hits a straight aortic segment at a velocity of 2m/s. The advanced model established in this master thesis eventually was compared with the aorta modeling approaches from current HBMs used in the field of crash safety. Last, the accident was reconstructed employing HBMs (CHARM-10yo and GHBMC-O F05), such to gain a better understanding of the loading mechanisms of the aorta in a belted occupant in a frontal impact.

The CEDATU analysis shows that in 2003 5% of all fatally injured occupants in traffic accidents in Austria died due to TRA. Compared to the UK and the USA, where about one fifth of all fatal injured in traffic accidents are due to TRA, the relevance in Austria was found to be lower. Among the 28 TRA-cases of CEDATU 10 were pedestrians and 18 were occupants. The location of rupture was documented in 20 cases. 90% of all ruptures are in the thoracic area of the aorta and 10% are in the

abdominal area of the aorta. The thoracic area can be divided into aortic arch (40%), descending thoracic aorta (35%) and heart valves/ascending aorta (15%).

For the FE simulations, the adapted material parameters (for intima, media and adventitia) show good accordance to biomechanical data for uni-axial extension tests. The material behavior in circumferential direction of the inflation test is satisfying; in axial direction significant deviations within the lower pressure range arise. The impact test shows an obvious variation of behavior concerning intrusion, deformation and strains compared to state-of-the-art aortic models. The reconstruction of the above mentioned accident with the GHBM shows a huge compression of the aorta (and the heart) around the thorax together with a pronounced traction between sternum and thoracic spine. This master thesis establishes the basis for the implementation of the improved model of the aorta for HBMs employed in the automotive industry.

Kurzfassung

Im Jahr 2009 starben drei Kinder an den Folgen einer Aortenruptur bei einem PKW-Frontalaufprall, obwohl sie gesetzeskonform in Kindersitzen auf der Rücksitzbank gesichert waren und die Geschwindigkeitsänderung als „überlebbar“ eingestuft wurde. Der Unfall wurde mit damaligen state-of-the-art Mehrkörpermodellen rekonstruiert. Zeitgemäße Finite Elemente Menschmodelle erlauben aber eine detaillierte Untersuchung der Mechanismen, die zu einer Aortenruptur führen, allerdings wird die Aorta in diesen Modellen stark vereinfacht.

Die Ziele dieser Masterarbeit sind es zunächst die Relevanz von Aortenrupturen bei Verkehrsunfällen in Österreich zu erheben, Theorien zu den Verletzungsmechanismen zusammenzufassen, Häufungsstellen von Rupturen zu ermitteln, den Unfall mit einem Menschmodell zu rekonstruieren, eine verbesserte Modellierung der Gefäßwand vorzustellen und dieses verbesserte Modell einem aktuellen Modell in seinem Verhalten gegenüberzustellen.

Fälle mit Aortenrupturen aus der CEDATU (Unfalldatenbank für detaillierte Analyse von Verkehrsunfällen in Österreich) wurden hinsichtlich Stelle der Ruptur, Alter, Geschlecht, Position im Fahrzeug, Unfallart und Verletzungsschwere analysiert.

Das Aortenmodell der Menschmodelle wurde verbessert. Im expliziten FEM-Löser LS-Dyna wurde ein hyperelastisches, anisotropes Materialmodell mit Dispersion ausgewählt, um die drei Schichten der Aorta (Intima, Media und Adventitia) zu modellieren. Die Materialparameter wurden mit der Optimierungssoftware Hyperstudy an vorhandene Daten von uni-axialen Tests angepasst. Anschließend wurde das Materialverhalten in Aufblas-Tests (Inflation-tests) mit experimentellen Daten verglichen. Es wird ein Impakt-Test durchgeführt, bei dem ein zylindrischer Impaktor mit 2m/s auf ein gerades Aortensegment prallt. Hier erfolgt ein Vergleich von einem herkömmlichen Modell, das im Bereich der Unfallsicherheit verwendet wird, mit dem verbesserten Modell aus dieser Masterarbeit. Zuletzt erfolgt die Nachstellung des eingangs erwähnten Unfalls mit zwei Menschmodellen (CHARM-10yo und GHBMCO F05).

Die CEDATU Ergebnisse zeigen, dass 2003 in Österreich bei Verkehrsunfällen 5% der tödlich verunglückten Insassen an einer Aortenruptur gestorben sind. Verglichen mit Großbritannien und den USA, wo TRA in beinahe einem Fünftel aller tödlichen Verkehrsunfälle auftritt, ist in Österreich die Relevanz deutlich geringer. Es wurden 28 Fälle von Personen, die TRA erlitten untersucht. Darunter waren 10 Fußgänger

und 18 Insassen. In 8 Fällen war der Bereich der Ruptur nicht dokumentiert. Bei den anderen 20 Fällen zeigt sich, dass 90% aller Rupturen im thorakalen Aortenbereich und nur 10% im Bereich des Abdomens liegen. Der thorakale Aortenbereich kann weiter unterteilt werden in Aortenbogen (40%), absteigende thorakale Aorta (35%) und Herzklappen/aufsteigende Aorta (15%).

Für die FE Simulationen zeigen die angepassten Materialparameter der einzelnen Schichten (Intima, Media und Adventitia) eine gute Übereinstimmung mit den biomechanischen Vergleichsdaten. Beim Aufblas-Test ist das Materialverhalten in Umfangsrichtung zufriedenstellend; in axialer Richtung treten im unteren Druckbereich starke Abweichungen auf. Der Impakt-Test zeigt eine deutliche Veränderung des Verhaltens hinsichtlich Eindringung, Verformungsbild und Dehnungen gegenüber herkömmlichen in HBM eingesetzten Aorten-Modellen. Die Nachstellung des eingangs erwähnten Unfalls mit dem GHBMC Menschmodell zeigte eine massive Komprimierung der Aorta (und des Herzens) im Bereich des Brustkorbs, zusammen mit einer Scherung zwischen Sternum und BWS. Die vorliegende Arbeit hat die notwendigen Grundlagen für die Implementierung des verbesserten Modells der Aorta in einem Menschmodell für die Automobilindustrie geschaffen.

Content

1	Introduction	1
1.1	Motivation	1
1.2	Objectives	2
1.3	Relevance	2
1.4	Anatomy and structure of the aorta	4
1.4.1	Layers of the aorta	5
1.5	Injuries of thorax and aorta in vehicle occupants	6
1.5.1	Rupture of the aorta	8
1.5.2	Spontaneous rupture of the aorta	8
1.5.3	Aortic aneurysm	8
1.5.4	Aortic dissection	8
1.6	Injury mechanism	9
1.6.1	Deceleration	10
1.6.2	Osseous pinch	10
1.6.3	Voigt's Shoveling	11
1.6.4	Water Hammer	11
1.7	Injury criteria	12
1.7.1	Thoracic trauma index (TTI)	12
1.7.2	Compression Criterion (C)	13
1.7.3	Viscous criteria (VC)	13
1.7.4	Combined thorax index (CTI)	14
1.8	Human Body Models	15
1.9	Modeling of arteries	17
1.9.1	Holzapfel model	20
1.9.2	Multi scale model	22
1.9.3	Freed-Einstein model	23
2	Method	27
2.1	Review of literature	27
2.2	Accident analysis	27

2.3	Uni-axial extension test.....	30
2.3.1	Matlab Model of Freed-Einstein Constitutive Model.....	30
2.3.2	LS-Dyna Single Element Model	33
2.4	Inflation test	34
2.5	Impact test	39
2.6	Full body impact	40
3	Results	43
3.1	Accident Analysis.....	43
3.1.1	CEDATU-cases with TRA.....	43
3.1.2	Occupant/pedestrian common overview.....	44
3.1.3	Occupant/Pedestrian: age groups	45
3.1.4	Occupants: time series.....	46
3.1.5	Pedestrians: time series.....	47
3.1.6	Location of TRA	48
3.1.7	Comparison CEDATU – Statistik Austria	49
3.2	Uni-axial extension test.....	50
3.3	Inflation test	52
3.4	Impact test	56
3.5	Full body impact.....	58
4	Discussion	61
4.1	Discussion of accident analysis results	61
4.2	Discussion of simulation results.....	64
5	Conclusion	67
6	List of figures.....	69
7	List of tables.....	71
8	References	72

1 Introduction

1.1 Motivation

In 2009 three children aged 5, 8 and 10 years involved in a full-frontal vehicle impact, which can be considered as survivable in terms of the estimated velocity change Δv , died at the accident scene. The children were seated in the rear and were properly restrained with seat belt and child seats (booster-seats). The accident has been reconstructed virtually and experimentally (multi body simulations, full vehicle crash test). For a more thorough understanding of the underlying injury mechanism, the accident shall be reconstructed with a detailed state-of-the-art finite element human body model (HBM). In current available human body models (GHBM, THUMS, CHARM-10), though, the aorta is simplified. Only linear elastic material models are used for the aortic wall and the fluid-structure-interaction is oversimplified as well. In some models the fluid remains unconsidered at all. Therefore it is necessary to enhance the modeling of the aorta previous to the reconstruction. In a preceding master thesis (Artner, 2016) different approaches for modeling the fluid and the fluid structure-interaction (FSI) were investigated.

This master thesis focuses on the modeling of the arterial wall: First, an appropriate material model that is already available in the explicit FEM solver LS-Dyna is selected. Second, material parameters are established based on uni-axial test data, for each of the three layers, namely 'Intima', 'Media' and 'Adventitia'. Third, the behavior of the material compound (Intima-Media, Adventitia, whole wall) in inflation tests is investigated, as well as the effect of various pre-strains (due to 'set-up' conditions) and initial strains (load-free configuration versus equilibrated configuration). Last, the wall model is merged with the FSI model which was established in the preceding master thesis.

In order to derive realistic loading conditions, the accident described above, is reconstructed by means of a child human body model (HBM). To gain a more thorough understanding on the epidemiology and the circumstances of TRA, the accident database CEDATU is analyzed concerning TRA-cases in Austria.

1.2 Objectives

The objectives of this master thesis are to answer the following questions:

- How relevant are aortic ruptures in accidents?
- Where are aortic injuries typically located?
- When does aortic rupture occur?
- Who is injured by TRA in traffic accidents?
- How could the aorta model in HBMs be enhanced?
- How does a modification of the material model affect the response of the aorta in case of an impact?

The answers should help to improve modeling of TRA in traffic accidents and to better understand the underlying injury mechanism by means of simulations.

1.3 Relevance

Traumatic rupture of the aorta (TRA) is a severe injury which is lethal in 97% of the cases. In UK and US TRA is responsible for more than one fifth of all fatalities. (Hardy et al., 2008; Richens et al., 2003)

The aortic isthmus, just under the outlet of the left subclavian artery, is by far the most common site of TRA. The aortic isthmus is connected to the thorax through ligaments and the head-neck vessels. After an impact the thorax follows a fast deceleration together with the aortic isthmus, whereas the viscous blood fluid still moves forward. The relatively large blood volume (an average male has about 5 to 6 liters blood, and approximately 30% of that is in the thorax) imposes relatively large inertial forces onto these restraints, leading to high shearing loads especially in the area of the bifurcation.

A complete rupture, which is a lethal injury in most cases, affects all wall layers of the artery. In case of a partial rupture some structures keep intact, bleeding occurs into a false lumen, which can burst at a later time. (Richens et al., 2002)

In a US hospital data about all patients, younger than 19 years with non-fatal blunt thoracic injuries, were collected over a period of 25 years. Out of 41 cases 11 children (aged 7 to 19 years) were selected for further investigation. It was found that

seven ruptures were located at thoracic aorta and the other four cases were located at the abdominal aorta. Most common mechanisms of injury were motor vehicle crashes. Looking at the use of restraint systems it was found that injuries to the abdominal aorta were seen with restrained children and injuries to the thoracic aorta were seen at those who were unrestrained. TRA in children often is associated with severe head and chest injuries, but in comparison to adults the higher survival rate is likely due to better stress response and less comorbidity. (Anderson et al., 2008; Gresik et al., 2013)

Another study concerning 40 children sustaining TRA shows as well that motor vehicle crashes are the leading mechanism of injury. (Escobar and Caty, 2011)

The overall mortality rate observed in children with aortic and great vessel injuries is 75%. Of these children, approximately 85% die at the scene and 15% die after arrival at the hospital. Fortunately, these injuries are seen quite seldom, i.e. in only 1% to 3% of all injured children. The most common and lethal of these injuries is traumatic aortic disruption. (Sadaghianloo et al., 2014)

Another study on the diagnosis and management of children with blunt injury of the chest shows that although thoracic injuries occur in only 4% to 6% of children hospitalized for trauma, they are responsible for up to 25% of pediatric trauma deaths. (Sartorelli and Vane, 2004)

In a study on fatal traffic accidents covering 664 analyzed cases in Budapest it was shown that among pedestrians and bicyclists there was a higher rate of head injuries (such as skull fractures, epidural hemorrhage, subdural hemorrhage, brain contusion) and injuries of the lower extremities. In occupants, though, thoracic and abdominal injuries, such as traumatic aortic rupture, hemothorax, and liver rupture were dominant. (Törő et al., 2005)

According to another study the age plays an important role in the anatomic distribution and severity of injuries and survival outcomes after pedestrian injuries. Thoracic aortic injury occurred in 0.3% of the analyzed cases. There were no aortic injuries in the age group 14 years or younger. It was shown that the risk for sustaining hemo-pneumothorax and rupture of the thoracic aorta increases significantly with age. (Demetriades et al., 2004)

1.4 Anatomy and structure of the aorta

The aorta is located in the thorax anterior to the trachea (windpipe) and esophagus (gullet). It originates from the left ventricle of the human heart and extends down to the abdomen, where it splits into the two common iliac arteries of the legs. The aorta can be divided into sections with respect to its course. First part is known as the ascending aorta, and then it rises to the aortic arch, which is the origin of the larger vessels, namely the brachiocephalic trunk, the left common carotid and the left subclavian artery. The aortic arch becomes the descending aorta at the height between fourth and fifth thoracic vertebrae, sometimes also referred as thoracic aorta. After the passage through the diaphragm it is called the abdominal aorta. (Lippert, 2010)



Figure 1.1: Heart with aorta in the human thorax (Gumpert, 2015)

The aortic isthmus is the part of the aortic arch distal to left subclavian artery and marks the area where the moveable arch and the fixed proximal descending thoracic aorta merge. Here the ligamentum arteriosum originates from the left pulmonary artery and leads to the descending aorta. In severe trauma this ligament restrains the aorta, inducing shear loads between the restrained and unrestrained sections, which might consequently result in TRA. (Chatterjee et al., 2012)

The main function of the aorta is the supply of the whole body with blood. The heart is supplied by branches of the ascending aorta. Head, neck and arms are supplied by branches of the aortic arch. The thorax is supplied by the descending aorta and branches of the abdominal aorta supply the abdomen, and pelvis and legs; as shown in Figure 1.2. (Lippert, 2010)

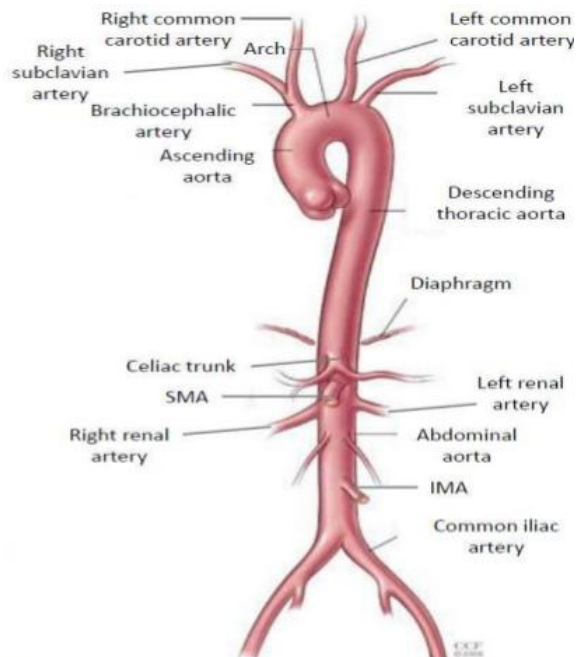


Figure 1.2: Anatomy of the aorta (Rakesh Sharma, 2014)

1.4.1 Layers of the aorta

The aorta wall is composed of three different layers: intima, media and adventitia (see Figure 1.3).

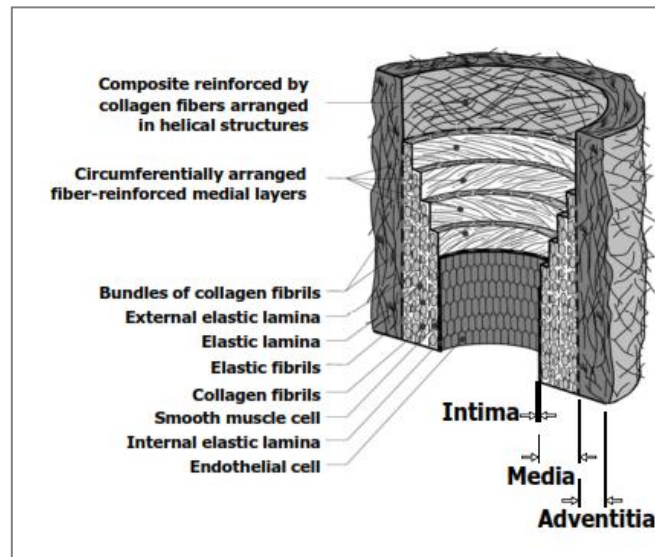


Figure 1.3: Different layers of the aorta (Holzapfel, 2003)

The inner layer is the intima. It is coated with endothelia cells, which inactivate the coagulation of blood and therefore act as solid-fluid interface. The intima is acting like a shear sensor and can affect the mechanic of the vessel. Contraction condition or growth behavior of the media muscle cells can be modified locally by means of endothelial cells release messengers, depending on shear forces induced by the flowing blood.

The middle layer is called media, which consists of a complex three-dimensional network of elastin, collagen and smooth muscle cells. Mechanical behavior of the entire vessel is strongly influenced and determined by orientations, distribution and contraction of these elements.

Adventitia is the outer layer, which acts like a shell, consisting mainly of collagen fibers and only a few elastin fibers. The adventitia has a highly deformable structure and acts as a overstretch protection of the two inner layers at non-physiological high pressure or axial tensions. (Holzapfel and Ogden, 2003)

1.5 Injuries of thorax and aorta in vehicle occupants

In general injuries of the thorax occur in frontal or side collisions. In many cases thorax injuries result from direct impacts with vehicle interior like the steering wheel, safety belts, doors or the dashboard. Most injuries result from blunt impacts. In general contusion results from compression and depends on corresponding compression velocity, whereas a laceration depends on size of compression. Figure 1.4 gives an overview of possible injuries and shows that TRA is one among several soft tissue injuries of the thorax. (Schmitt et al., 2010)

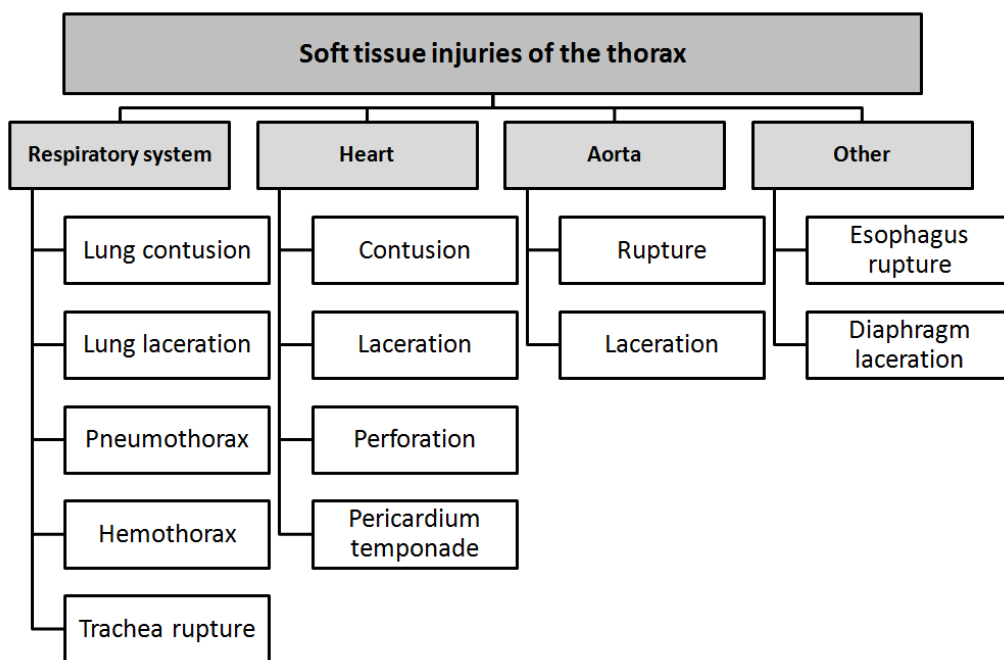


Figure 1.4: Possible injuries of soft tissue of the thorax (Schmitt et al., 2010)

Injuries of the thorax categorized according to abbreviated injury scale (AIS) are summarized in the in the table below.

Table 1.1: AIS severity of thorax injuries (Schmitt et al., 2010)

AIS	severity	soft tissue	skeleton
1	minor	skin abrasion, contusion or minor laceration	1 rip fracture
2	moderate	major skin abrasions	2-3 rip fractures
3	serious	minor heart contusion, one-sided lung contusion	less than 3 rip fractures on one side and less than 4 rip fractures on the other one, 2-3 rip fractures with hemo- or pneumothorax
4	severe	major heart contusion, rupture of aortic intima	more than 4 rip fractures on both sides, more than 4 rip fractures unilateral with hemothorax or pneumothorax, instable thorax
5	critical	severe injury of aorta, perforation of heart, ventricular rupture of heart	instable thorax on both sides
6	maximum	aortic rupture with hemorrhage, which is not limited to the mediastinum	-
9	NFS	not further specified	-

1.5.1 Rupture of the aorta

At a TRA locally occur such high mechanical forces that the healthy vessel layer ruptures. A complete rupture affects all wall layers of the artery, whereas in a partial rupture some structures keep intact and bleeding occurs only between the layers. TRA injury mechanisms are described in detail in an appropriate sub item. (Richens et al., 2002)

1.5.2 Spontaneous rupture of the aorta

Spontaneous rupture of the aorta without trauma, aneurysm or dissection is extremely rare, though a small intramural hematoma with ruptured arteriosclerotic plaque can be clinically interpreted as 'spontaneous' aortic rupture as well. However, for the distinction between spontaneous aortic rupture and aortic rupture due to penetrating arteriosclerotic ulcer precise histopathologic studies are necessary. (Yokoyama et al., 2000)

1.5.3 Aortic aneurysm

An aneurysm indicates the widening of an arterial blood vessel by at least 50%. If all wall layers are affected it is a real (verum) aneurysm otherwise it is a false one. Due to loss of elasticity of media vessel layer, it cannot resist the intravascular pressure anymore. (Schreiber et al., 2006)

1.5.4 Aortic dissection

A dissection of aorta occurs if only the intima vessel layer ruptures and blood can flow into the media layer of the vessel. As the blood is under high pressure, the blood penetrates the diseased media and cleaves it longitudinally, eventually dissecting the aortic wall. Functionally the space between the dissected layer from a second lumen, called a 'false' lumen. The site of the ruptured intima is called entry, where the blood flows into the so called false lumen. Often the blood flows back into the true lumen through a re-entry site. (Eichinger et al., 2001)

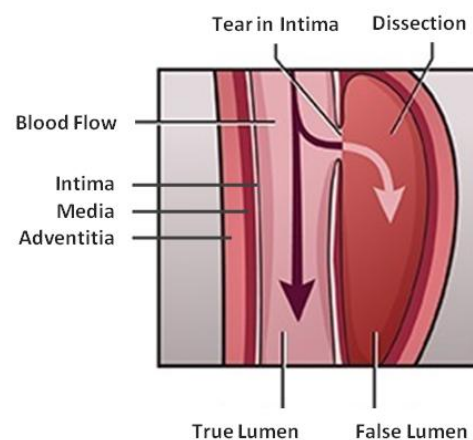


Figure 1.5: Blood Flow into false lumen - aortic dissection (adopted from U.S. National Library of Medicine)

1.6 Injury mechanism

The injury mechanism describes the circumstances which lead to an injury. It is used to estimate the involved forces as well as the potential severity for fractures or internal organ damage that a person may suffer. (Med Dict, 2015)

Injuries of the thorax in traffic accidents mostly occur due to an impact with a blunt or plane objects without penetration into tissue. Three different injury mechanisms can be distinguished concerning a blunt impact of the thorax. First compression, second viscous loads and third loads due to inertia. Certainly combinations of these three mechanisms can occur as well. Whereas mechanisms leading to rib fractures or lung injuries are relatively well understood the mechanisms leading to injuries of other thoracic organs are less well understood and need further investigations. (Schmitt et al., 2010)

There have been postulated several mechanisms why the isthmus region is the most common site of aortic rupture; a combination of an abrupt deceleration leading to high velocity changes, a sudden chest compression (e.g. caused by hyperflexion of the spine) and the traction on the aortic isthmus counts to the most accepted theories. Other theories suggest mechanisms known as 'shoveling effect', 'osseous pinch' and 'water-hammer' effect, which are described more thoroughly below. (Benjamin and Roberts, 2012)

The figure below shows where forces in a blunt traumatic injury are acting on the aortic arch.

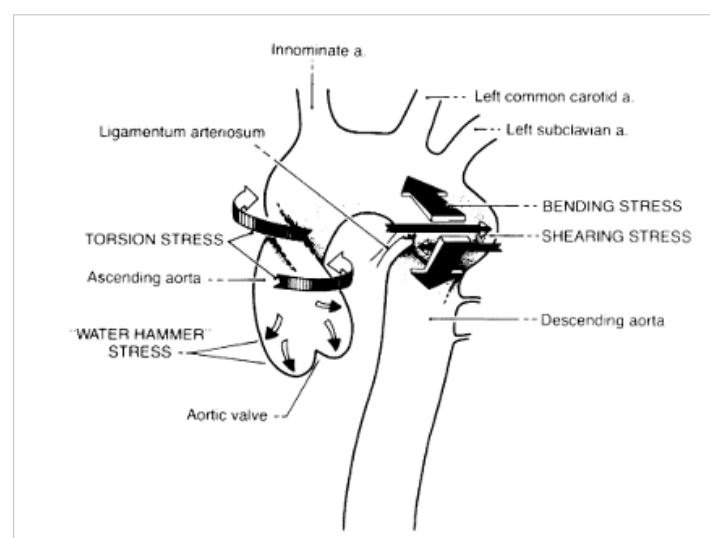


Figure 1.6: Putative forces acting on the aorta during blunt traumatic injury (Richens et al., 2002)

1.6.1 Deceleration

The deceleration mechanism can be distinguished into horizontal deceleration, which occurs in traffic accidents and vertical deceleration, which occurs in drops from a certain height. The required force to rupture the vessel through a deceleration of heart and aorta is estimated to be 77g related to the weight of heart and aorta. A fall from a height of between 10m and 15m lead to critical vertical deceleration potentially causing TRA. A fall on the flat back is even more critical, as the available 'crush' displacement amounts for 10cm or less. That means that the critical drop height is reduced to between 2m and 5m. Horizontal deceleration alone may not be sufficient for aortic rupture as the possible deceleration displacement is 50cm due to deformable vehicle parts. Assuming 10cm of 'human deceleration displacement', the critical impact velocity for traffic accidents related TRA is estimated 300km/h, which hardly occurs in road traffic. (Zehnder, 1960)

1.6.2 Osseous pinch

In the osseous pinch the aorta is encased by the anterior thoracic bony structures (like sternum, clavicle and first rib) and the vertebral column. In blunt thoracic trauma compressive forces depress the anterior osseous structures, causing them to rotate posteriorly and inferiorly about the posterior rib articulations. This leads to pinching and shearing of vascular structures, which are posed in between the anterior and posterior bony structures. (Crass et al., 1990)

The figure below shows the relationship of aorta to anterior osseous complex and spine. The arrows indicate the movement of clavicle, sternum and anterior ends of the first rib that occurs during frontal impact with full compression. The site of expected aortic impingement is shown at the upper arrow with a small asterisk. (Cohen et al., 1992)

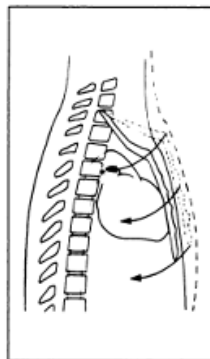


Figure 1.7: Line drawing of osseous pinch mechanism (Cohen et al., 1992)

1.6.3 Voigt's Shoveling

The 'Voigt's Shoveling' effect is known as a mechanism where the sternum is forced back against the spine, and the inflexion of the sternum shoveled mediastinal soft tissues toward the upper thoracic aperture. (Voigt and Wilfert, 1969)

'Voigt's Shoveling' involves dorso-cranial motion of the heart in response to frontal impact to the abdomen and thorax. This type of motion tends to place the aorta in tension, either by upward movement of the mediastinal contents in general or by fulcrum action of the hilum of lungs. The level and direction of impact, particularly the angle in the sagittal plane, will greatly influence the result. (Shah, 2007)

Cross-sectional views of the thorax, showing forces causing aortic injury according to the theory of the shoveling mechanism are shown in the figure below.

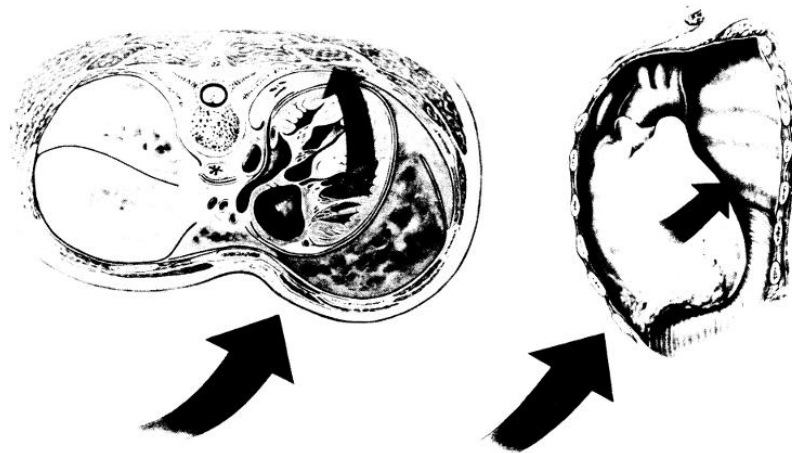


Figure 1.8: Cross-sectional views of the thorax, showing forces causing aortic injury according to the theory of the 'shoveling' mechanism. (Tribble and Crosby, 1988)

1.6.4 Water Hammer

This mechanism can be explained with following example. The blood in the aortic arch will continue forwards due to its inertia if a person is suddenly stopped during forward movement. This sudden change of momentum is causing a hydraulic shock loading the anterior wall of the ascending aorta and causing traction on the posterior wall in the isthmus region. (Lundevall, 1964)

1.7 Injury criteria

Injuries of the thorax result from compression, loads due to viscosity and inertia of thorax as well as combinations of the same. By means of injury criteria (IC) the biomechanical behavior of the thorax under load as well as appropriate injury induced tolerance values can be determined. More precisely ICs assign certain loads of the thorax to a corresponding risk of injury. Several criteria are introduced and listed with advantages and disadvantages. (Schmitt et al., 2010)

1.7.1 Thoracic trauma index (TTI)

This IC was introduced for the evaluation of side impact collisions. The assumption was that occurrence of injury depends on the average of maximum side acceleration of the thorax and the acceleration of the lower thoracic spine, as well as age and weight of person. TTI criterion has the dimension [g] and is defined as follows:

$$TTI = 1,4AGE + 0.5 (RIB_y + T12_y)(M / M_{std})$$

AGE	Age of person in years
RIB_y	Maximum of absolute value of lateral acceleration between 4 th and 8 th rib on the impact side
$T12_y$	Maximum of absolute value of lateral acceleration at 12 th thoracic vertebra
M	Mass of the test subject (PMHS) in kilogram
M_{std}	Reference mass of person with 75 kilogram

A different version of the TTI, called TTI(d) is calculated when using a 50th percentile Hybrid III dummy to perform crash tests. The age related term is omitted and the mass ratio becomes 1.0. It needs to be determined previous to the testing procedure whether TTI or TTI(d) is calculated as the acceleration signals have to be pre-processed.

TTI reflects more a statistical correlation as a biomechanical; in particular there is no direct reference to an injury mechanism. (Schmitt et al., 2010)

1.7.2 Compression Criterion (C)

The maximum thorax compression correlates better with the AIS classification of injuries than force and acceleration do. The compression is defined as deformation of chest (in millimeters) divided by thickness of thorax (in millimeters).

$$AIS = -3.78 + 19.56 C$$

A compression of 40% (thorax deflection of 92mm divided by a thorax thickness of 230mm) results in an AIS 4 injury, whereas a compression of 30% only results in an AIS 2 injury. For the 50th percentile Hybrid III dummy in frontal impact a maximum deflection of 76mm is allowed. (Schmitt et al., 2010)

1.7.3 Viscous criteria (VC)

The VC considers that soft tissue injuries not only depend on compression but also on the velocity of compression. The VC value describes the maximum of the time-dependent product of deformation velocity and deformation of the thorax. Both parameters are determined by measuring of rib compression in case of side impact and chest compression in case of frontal impact, respectively. (Schmitt et al., 2010)

$$VC = V(t) \times C(t) = \frac{d[D(t)]}{dt} \times \frac{D(t)}{b}$$

$V(t)$ velocity of deformation [m/sec], calculated by differentiation of deformation $D(t)$

$C(t)$ function of compression, defined as ratio of deformation $D(t)$ and thickness of thorax at the beginning b

Table 1.2: Frontal impact tolerances of the chest for viscous criteria (Nahum and Melvin, 2002)

VC (unit: m/sec)	Injury Level
1.0	25% probability of AIS \geq 4
1.3	50% probability of AIS \geq 4

1.7.4 Combined thorax index (CTI)

The CTI is another IC for thorax under frontal loads. It is a combination of compression and acceleration; particularly with regard to the distinctive loads by airbags and restraint systems. The CTI is defined as a 3ms value of the resulting acceleration of the spine and the thorax deformation.

$$CTI = \frac{A_{max}}{A_{int}} \times \frac{D_{max}}{D_{int}}$$

A_{max} 3ms value of the resulting spine acceleration [g],

A_{int} critical 3ms reference value

D_{max} compression of the chest [mm]

D_{int} critical compression value

Whereas the maximum thorax acceleration is a measurement for load of all resulting forces in general, the thorax compression is an indicator for the load converted by the safety belt. The higher compression is per unit of acceleration the higher is the relative part of the restraint system. (Schmitt et al., 2010)

Table 1.3: Frontal impact tolerance of the chest for the combined thorax index (Nahum and Melvin, 2002)

CTI	Injury Level
Amax: 60.0 g Dmax: 76 mm	50% probability of AIS > 3



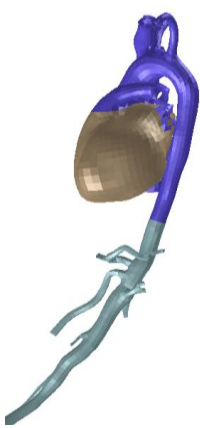

Table 1.4: Advantages and disadvantages of each criteria

Criteria	Advantage	Disadvantage	Valid for
TTI	evaluation of side impact collisions	more a statistical than biomechanical correlation, no direct reference to an injury mechanism	PMHS
CC	compression correlates better with AIS than force and acceleration do	high-speed impact can cause severe injury even before tolerance limit is reached	Hybrid III
VC	velocity of compression is considered		PMHS
CTI	compression and acceleration are combined	only for frontal impacts	PMHS

1.8 Human Body Models

The next step was a comparison of different human body models with regard to the aorta. In table 1.5 are shown four models: The total human model for safety of an adult 5th percentile female (THUMS-AF05), the collaborative human advanced research model of a 10 year old child (CHARM-10), the global human body models consortium of an adult 50th percentile male (GHBMC-M50) and of an adult 5th percentile female (GHBMC-F05). The criteria were body measurements, which are approximations to the statistical data of NHTSA (2015) as well as the anatomy of aorta and aortic arch. The licenses are present for each single model.

Table 1.5: Comparison of different aortic models of HBM-occupants

THUMS-AF05	CHARM-10	GHBMC-M50	GHBMC-F05
5 th percentile female	10 year old child	50 th percentile male	5 th percentile female
150 centimeters	140.1 centimeters	175 centimeters	152 centimeters
49 kilogram	35 kilogram	76.9 kilogram	51 kilogram
			
Accordance to anatomy			
brachiocephalic artery, left common carotid artery and left subclavian artery neglected	descending aorta ends in abdominal area	detailed anatomy	detailed anatomy
Modeling of the vessel wall layers			
2D shell of one layer	2D shell of one layer	2D shell of one layer	
*MAT_FABRIC RO: 1.0E-09 EA: 2.56 PRBA: 0.35 CSE: 1.0 DAMP: 1.0 FORM: 1.0	*MAT_ELASTIC RO: 1.0000E-06 E: 8.8700E-03 PR: 0.4	*MAT_VISCOELASTIC RO: 1.0000E-06 BULK: 3.333E-03 GO: 3.448E-04 GI: 6.896E-05 BETA: 0.25	

Modeling of the arterial blood		
3D solid fluid	3D solid fluid	Airbag fluid
*MAT_ELASTIC_FLUID	*MAT_ELASTIC_FLUID	*AIRBAG_LINEAR_FLUID
RO: 1.0E-09	RO: 1.0000E-06	VSCA: 1.0000
E: 0.0	E: 0.0	PSCA: 1.0000
PR: 0.0	PR: 0.45	MWD: 0.5
VC: 0.1	VC: 0.21	SPSF: 0.1000
CP: 0.0	CP: 0.67E-05	BULK: 1.000E-03
		RO: 1.000E-06

***MAT_ELASTIC**

This is an isotropic hypoelastic material and the specialization of this material allows the modeling of fluids (see parameters of *MAT_ELASTIC_FLUID below).

RO: Mass density

E: Young's modulus

PR: Poisson's ratio

***MAT_FABRIC**

This material is especially developed for airbag materials. The fabric model is a variation on the layered orthotropic composite model of *MAT_022 in LS-Dyna.

EA: Young's modulus – longitudinal direction. For an isotropic elastic fabric material only EA and PRBA are defined and used as the isotropic Young's modulus and Poisson's ratio, respectively.

PRBA: Minor Poisson's ratio b-a direction.

CSE: Compressive stress elimination option. (1.0 = eliminate compressive stresses)

DAMP: Rayleigh damping coefficient

FORM: Flag to modify membrane formulation for fabric material. (1.0 = invariant local membrane coordinate system)

***MAT_ELASTIC_FLUID**

VC: Tensor viscosity coefficient

CP: Cavitation pressure

***MAT_VISCOELASTIC**

This model allows the modeling of viscoelastic behavior.

RO: Mass density

BULK: Elastic bulk modulus

G0: Short-time shear modulus

G1: Long-time (infinite) shear modulus

BETA: Decay constant

***AIRBAG_LINEAR_FLUID**

This model provides a way of defining thermodynamic behavior of the gas flow into the airbag as well as a reference configuration for the fully inflated bag. The purpose besides defining an airbag is defining a control volume.

VSCA: Volume scale factor

PSCA: Pressure scale factor

MWD: Mass weighted damping factor

SPSF: Stagnation pressure scale factor

BULK: Bulk modulus of the fluid in the control volume

RO: Density of the fluid

1.9 Modeling of arteries

In a study conducted by the Institute of Biomechanics at Graz University of Technology material models for arterial tissue were summarized and compared (see below). The majority of constitutive models are phenomenological in nature and do not take into account directly the histological structure. These models are summarized in the following table with the strain energy function, needed material parameters, information about which kind of tissue was used in experiments, modeled layers as well as information and restrictions of the model. (Holzapfel et al., 2000)

Table 1.6: Overview of phenomenological models for arterial tissue

isotropic rubber-like model for carotid arteries (proposed by Delfino et al., 1997)	
strain-energy function	$\bar{\Psi} = \frac{a}{b} \left\{ \exp \left[\frac{b}{a} (\bar{I}_1 - 3) \right] - 1 \right\}$
material parameters	a = 44.2 [kPa] b = 16.7 [-]
experimental data	human carotid artery
layers	thick-walled tube
short information	is able to model the typical stiffening effects at high pressures
restrictions	oversimplification through use of isotropy
exponential model of Fung's Type (proposed by Humphrey, 1999)	
strain-energy function	$\bar{\Psi} = \frac{1}{2} c [\exp(Q) - 1]$ Q is defined by several non-dimensional material parameters ($b_1 \dots b_9$), and components of the modified Green-Lagrange strain tensor (referred to cylindrical polar coordinates)
material parameters	c = 26.95 [kPa] b ₁ = 0.9925 [-] b ₂ = 0.4180 [-] b ₃ = 0.0089 [-] b ₄ = 0.0749 [-] b ₅ = 0.0295 [-] b ₆ = 0.0193 [-] b ₇ = 5.0000 [-]
experimental data	carotid artery of a rabbit
layers	thick-walled tube
short information	is suitable for arbitrary (three-dimensional) states of deformations
restrictions	the 'physical' meanings of the individual parameters are unclear, formulation associated with geometrical simplifications, not suitable for analysis of the through-thickness stress distribution

polynomial model (proposed by Vaishnav et al., 1973)			
strain-energy function	$\hat{\Psi} = c_1 \bar{E}^2_{\theta\theta} + c_2 \bar{E}_{\theta\theta} \bar{E}_{ZZ} + c_3 \bar{E}^2_{ZZ} + c_4 \bar{E}^3_{\theta\theta} + c_5 \bar{E}^2_{\theta\theta} \bar{E}_{ZZ} + c_6 \bar{E}_{\theta\theta} \bar{E}^2_{ZZ} + c_7 \bar{E}^3_{ZZ}$		
material parameters	<table style="width: 100%; border: none;"> <tr> <td style="width: 50%; border: none;"> $c_1 = -24.385$ [kPa] $c_2 = -3.589$ [kPa] $c_3 = -1.982$ [kPa] $c_4 = 46.334$ [kPa] </td> <td style="width: 50%; border: none;"> $c_5 = 32.321$ [kPa] $c_6 = 3.743$ [kPa] $c_7 = 3.266$ [kPa] </td> </tr> </table>	$c_1 = -24.385$ [kPa] $c_2 = -3.589$ [kPa] $c_3 = -1.982$ [kPa] $c_4 = 46.334$ [kPa]	$c_5 = 32.321$ [kPa] $c_6 = 3.743$ [kPa] $c_7 = 3.266$ [kPa]
$c_1 = -24.385$ [kPa] $c_2 = -3.589$ [kPa] $c_3 = -1.982$ [kPa] $c_4 = 46.334$ [kPa]	$c_5 = 32.321$ [kPa] $c_6 = 3.743$ [kPa] $c_7 = 3.266$ [kPa]		
experimental data	canine thoracic aorta, rabbit carotid arteries		
layers	thick-walled cylindrical tube of incompressible material		
short information	three-parameter model is too inaccurate for a serious investigation, the twelve-parameter model has no significant advantage over the seven-parameter model it is acceptable in the tensile region ($\bar{E}_{\theta\theta} > 0$, $\bar{E}_{ZZ} > 0$)		
restrictions	due to the cubic nature of the strain-energy function, it is not convex for any set of values of the material parameters		
two-dimensional exponential model (proposed by Fung et al., 1979)			
strain-energy function	$\hat{\Psi} = \frac{1}{2} c [\exp(\hat{Q}) - 1]$ $\hat{Q} = b_1 \bar{E}^2_{\theta\theta} + b_2 \bar{E}^2_{ZZ} + 2b_4 \bar{E}_{\theta\theta} \bar{E}_{ZZ}$		
material parameters	<table style="width: 100%; border: none;"> <tr> <td style="width: 50%; border: none;"> $c = 28.58$ [kPa] $b_1 = 0.8329$ [-] </td> <td style="width: 50%; border: none;"> $b_2 = 0.6004$ [-] $b_4 = 0.0169$ [-] </td> </tr> </table>	$c = 28.58$ [kPa] $b_1 = 0.8329$ [-]	$b_2 = 0.6004$ [-] $b_4 = 0.0169$ [-]
$c = 28.58$ [kPa] $b_1 = 0.8329$ [-]	$b_2 = 0.6004$ [-] $b_4 = 0.0169$ [-]		
experimental data	dog carotid artery		
layers	thick-walled tube of incompressible material		
short information	is able to model the basic characteristics of the mechanical behavior of arteries except at low pressures		
restrictions	the inner radius is independent of the axial stretch when internal pressure is zero, and a strong influence of the residual stresses on the pressure – radius behavior is observed		

two-dimensional logarithmic model (proposed by Takamizawa and Hayashi, 1987)					
strain-energy function	$\hat{\Psi} = -c \ln(1 - \psi)$ $\psi = \frac{1}{2} b_1 \bar{E}^2_{\theta\theta} + \frac{1}{2} b_2 \bar{E}^2_{ZZ} + b_4 \bar{E}_{\theta\theta} \bar{E}_{ZZ}$				
material parameters	<table border="1" style="width: 100%; border-collapse: collapse;"> <tr> <td style="padding: 2px;">c = 57.94 [kPa]</td> <td style="padding: 2px;">b₂ = 0.4728 [-]</td> </tr> <tr> <td style="padding: 2px;">b₁ = 0.6311 [-]</td> <td style="padding: 2px;">b₄ = 0.0301 [-]</td> </tr> </table>	c = 57.94 [kPa]	b ₂ = 0.4728 [-]	b ₁ = 0.6311 [-]	b ₄ = 0.0301 [-]
c = 57.94 [kPa]	b ₂ = 0.4728 [-]				
b ₁ = 0.6311 [-]	b ₄ = 0.0301 [-]				
experimental data	dog carotid artery				
layers	thick-walled tube of incompressible material				
short information	is able to represent the typical response of arteries quite well expect at low pressures				
restrictions	only applicable for a limited range of states of deformation				

1.9.1 Holzapfel model

This model captures the artery as a thick-walled nonlinearly elastic circular cylindrical tube, which consist of two layers: media and adventitia, which are mechanically relevant in healthy tissue. The model requires only three material parameters for each layer and is used to study the response of an artery under combined axial extension, inflation and torsion. These material parameters try to include the histological structure of arterial walls, like fiber directions.

Each layer is modeled with a separate strain-energy function and a different set of material parameters. The strain-energy function is split into a part with isotropic deformations and a part with anisotropic deformations. It is assumed that the mechanical response of the non-collagenous matrix material contributes to isotropic part and that fibers contribute to the anisotropic part as the resistance to stretch at high pressures is due to collagenous fibers.

$\bar{\Psi}(\bar{C}, A_1, A_2) = \frac{c}{2}(\bar{I}_1 - 3) + \frac{k_1}{2k_2} \sum_{i=4,6} \{ \exp[k_2(\bar{I}_i - 1)^2] - 1 \}$		
The isochoric strain energy function of the arterial wall consists of an...	isotropic term for the matrix material and an...	anisotropic term for the collagenous fibers.

\bar{C} ... deformation measure

A_1, A_2 ... Tensors, which are defined as the tensor products of the two reference direction vectors (families of collagenous fibers are characterized by these direction tensors)

I_1, \dots Invariant, which measures the trace of \bar{C}

I_4, I_6 ... Invariants, which are stretch measures for the two fiber families

c ... stress-like material parameter ($c > 0$)

k_1 ... stress-like material parameter ($k > 0$)

k_2 ... dimensionless parameter

k_1 and k_2 enable modeling of the histological-based assumption, that the collagen fibers do not influence the mechanical response of the artery at low pressures.

As this approach approximates the arterial wall as two-layer thick-walled tube with each layer modeled as a highly deformable fiber-reinforced composite it leads to a fully three-dimensional anisotropic material description incorporating histological information. This model is consistent with both mechanical and mathematical requirements and suitable for use of finite element methods. It enables insight into the nature of the stress distribution across the arterial wall and for a detailed study of the mechanical functionality of arteries. (Holzapfel et al., 2000)

1.9.2 Multi scale model

Mechanical constitutive models with integrated structural information can be helpful to better understand its mechanical behavior in physiological and pathological conditions.

(Weisbecker et al., 2015) propose a multi scale model, which is able to capture the nonlinear and anisotropic behavior of the aortic layers in three different scales, including the waviness:

- A single collagen fiber
- Bundle of collagen fibers
- Collagen network within the tissue

The two parameters, which are used by the model, are a shear modulus (μ_m) of the isotropic matrix material and a stiffness parameter (μ_f) related to a single collagen fiber. The bivariant von Mises distribution is used to describe the three-dimensional distribution of the collagen fibers, as well as it is fitted to experimental data from uniaxial tensile tests with the MATLAB function **lsqnonlin**. After this first fit, the parameters of the Cauchy stress tensor are identified as well.

The transformation from the reference configuration to the current configuration is described with the deformation gradient F . The volume ratio J ($= \det F$) is 1 for an incompressible deformation. The orientation of a fiber is represented by an arbitrary direction vector M . That contains a polar and a azimuth angle corresponding to in plane and out of plane angles, respectively.

A single collagen fiber contributes to the strain-energy function only when it is stretched after it is uncrimped, also called recruited. In a bundle of fibers it is used a beta function which is defined in the interval between the stretch at which the first fiber is recruited and the stretch at which the last fiber is recruited. The relative density of fibers in a specific direction is described in the orientation distribution function $\rho(M)$ and for isotropy it is 1. The strain energy of the tissue consists of a term with the volume fraction and shear modulus of the matrix as well as the total strain energy per unit reference volume for all collagen fibers in the tissue. As both terms are functions of the right Cauchy-Green tensor C , this is how the equation depends on the deformation.

$\Psi(C, M) = (1 - \nu) \frac{\mu_m}{2} (I_1 - 3) + n \int_{\Omega} \rho(M) w_b(\lambda) d\Omega$		
The strain energy function of the tissue consists of a...	term for the matrix material and a...	term for the collagen fibers.

After fitting process, the parameters got changed to check the sensitivity of the model. In the paper can be seen details in the single diagrams. The mean Young's modulus for the individual collagen fibers is $E = 54.3$ MPa and it can be obtained a μ_f of $5.22 \text{mN } \mu\text{m}$. The λ_1 is set 1, as they assumed that some fibers may be recruited immediately after initiation of loading. The anisotropic model is very sensitive to the mean fiber angle α and the before mentioned λ_1 . The sensitivity curves of μ_f and η match exactly, which means that these parameters are linearly dependent. (Weisbecker et al., 2015)

1.9.3 Freed-Einstein model

The following explained model is the only appropriate one, which is already implemented in LS-Dyna.

The single terms of the formula of the Freed-Einstein-Model consists of three parts: a volumetric part (dilatation), an isotropic deviatoric part and an anisotropic deviatoric part.

<i>Hydrostatic term (HT):</i>	$\kappa J(J - 1)C^{-1} + \dots$
-------------------------------	---------------------------------

This term describes the volumetric changes.

Kappa.... compression modulus

J.... Jacobi-determinant calculated from $\det(F)$, where F = deformation gradient

C... right Cauchy-green deformation tensor; can be calculated from F .

<i>Isotropic term (IT):</i>	$\dots \mu J^{-\frac{2}{3}} \mathbf{DEV} \left[\frac{1}{4} (\mathbf{I} - \bar{\mathbf{C}}^{-2}) \right] \dots$
-----------------------------	---

That term describes the part of tensions without change of volume.

μ ... isotropic shear modulus that models elastin ($\mu \dots = 0.5$: *kappa* would get infinite and J would become zero, so this term would be dropped, therefore following assumption is made $\mu = 0.497$)

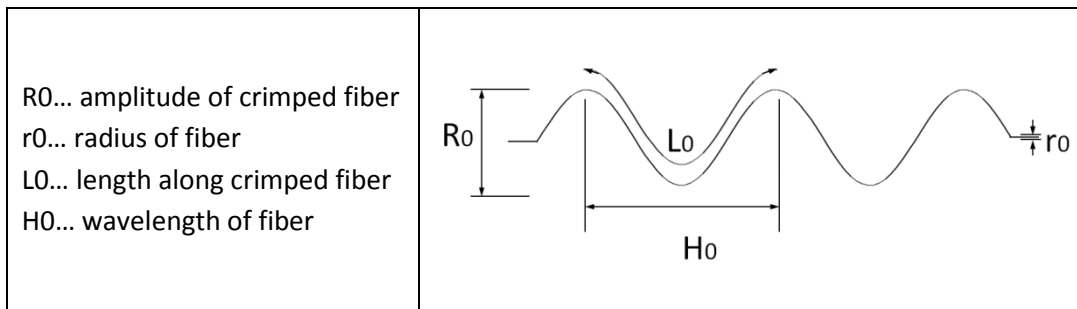
I... unit tensor

$\bar{\mathbf{C}}$... isochoric part of the Cauchy-green deformation tensor

<i>Anisotropic part (AT):</i>	$\dots J^{-\frac{2}{3}} \sum_{i=1}^n [\sigma_i(\lambda_i) + \varepsilon_i(\lambda_i)] \mathbf{DEV}[\mathbf{K}_i]$
-------------------------------	---

That part describes the fiber-reinforced Neo-Hook-model.

σ_i ... describes a 1D-fiber with parameters R_0 , r_0 , L_0 , H_0 ; these are also needed to calculate the passive fiber model parameters C_1 , C_2 and C_3 .



λ_i ... describes how much of the real strain is applied onto the fiber; this is calculated by means of $tr[KC]$

K_i ... dispersion tensor (or anisotropy tensor); the passive and active fiber models are defined in the fiber coordinate system. The dispersion tensor rotates and weights these one-dimensional models, so both then are described in the three-dimensionality and in the global coordinate system.

Beta... angle to describe the mean fiber direction

Theta... angle to describe position of fiber families depending on mean fiber direction assuming that there are two fiber families

Delta... angle to describe dispersion of single fibers of a fiber family

F ... fiber dispersion parameter, describes the extent of fibers to the third dimension; three different conditions are possible:

$F = 1$: fiber-splay (2D) in x-y-direction (normal to membrane is gamma)

$F = 0$: fiber-splay (2D) in z-direction (normal to membrane is beta)

$F = 0.5$: fiber-splay (3D) in all three directions with transverse isotropy

The next figure shows fiber dispersion with the above mentioned angles as well as the fiber dispersion parameter F .

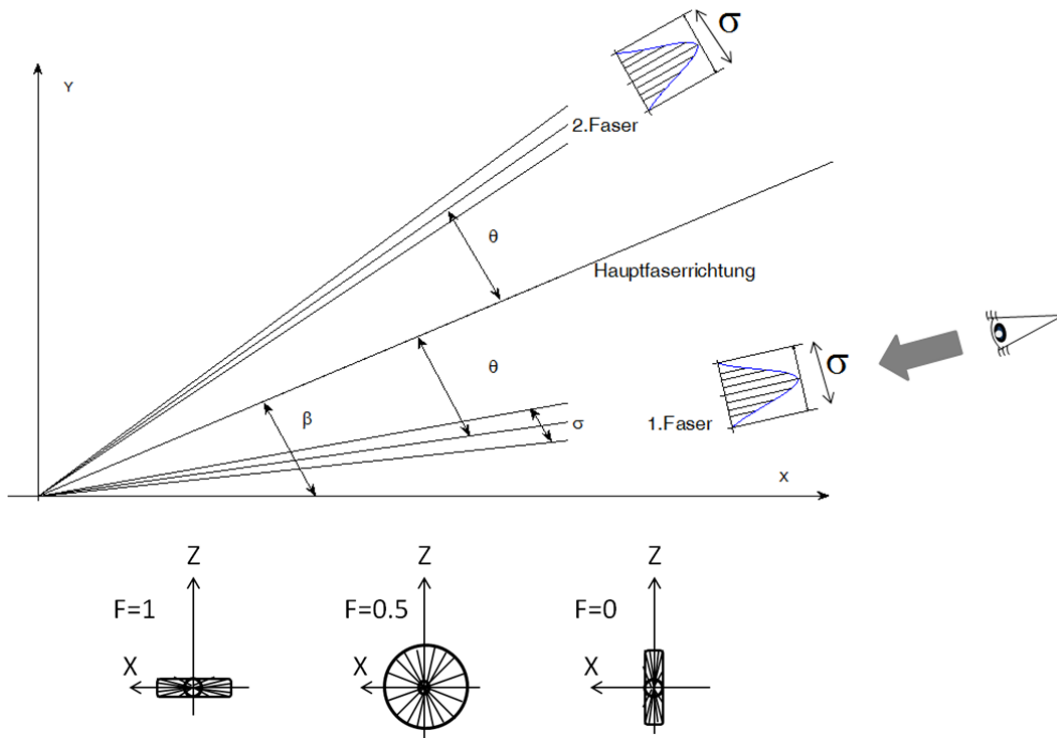


Figure 1.9: Draft of the mean fiber direction with 2 fiber families and the fiber dispersion parameter F

The difference between the Freed-Einstein model and the Neo-Hook model is in the first two terms. The anisotropic term is the same like at the Freed-Einstein model. The calculation of hydrostatic and isotropic term at the Neo-Hook model is as follows:

<i>Hydrostatic term (HT):</i>	$J^{-1}(\lambda * \log J - \mu)I + \dots$
-------------------------------	---

J... Jacobi-determinant calculated from $\det(F)$, where F = deformation gradient

I... unit tensor

λ ... 1. Lamè parameter

<i>Isotropic term (IT):</i>	$\dots J^{-1} * \mu * B \dots$
-----------------------------	--------------------------------

B... left Cauchy-green deformation tensor; can be calculated from F .

The first Lamè parameter can be calculated as follows:

<i>1. Lamè parameter</i>	$\lambda = \frac{2 * \mu * \nu}{(1 - 2 * \nu)}$
--------------------------	---

2 Method

2.1 Review of literature

First of all a review of the literature is realized to get a general idea of relevant papers and the state of the art. Main keywords have been aortic rupture, traumatic rupture of the aorta, aortic rupture in traffic accidents, pediatric aortic rupture, children/adolescents with aortic rupture, pedestrian with aortic rupture, and location of traumatic rupture of the aorta. Beside papers of different internet sources also the papers of IRCOBI conference of the past decades have been included in search.

2.2 Accident analysis

An accident analysis has been realized with data of CEDATU (Central Database for In-Depth Accident Study in Austria) as well as statistical data of Statistik Austria.

The CEDATU is a central database of fatalities in Austria, which was initiated by TU Graz to collect different accident configurations. In addition to information regarding vehicle and infrastructure CEDATU also has detailed information on the casualties. (Steffan and Tomasch, 2006)

The injuries are AIS (abbreviated injury scale) coded. AIS is a standardized system for categorizing injury type and severity with a simple numerical method for ranking and comparing injuries. The AIS is based on anatomical injury and scores the severity of the injury itself, but not the consequences of the injuries. The AIS classifies individual injuries by body region on a scale ranging from AIS 1 (minor) to AIS 6 (currently untreatable). Each injury is assigned a 6-digit numerical code with the AIS severity score. From left to right these are body region, type of anatomical structure, specific anatomical structure and level. The level of thorax injuries was further explained in sub-chapter 1.5 Injuries of thorax and aorta.

The cases registered in CEDATU were inquired for TRA-injuries, which means body region thorax (4) and abdomen (5), type of anatomical structure vessels (2), specific anatomical structure vessels (02) and several levels (06, 08, 10, 16, 18, 99). Therefore the following AIS-Codes have been included:

Table 2.1: Used AIS-Codes for accident analysis in CEDATU

Body region	Type of anatomical structure	Specific anatomical structure		Level		.	AIS
4	2	0	2	0	6	.	4
4	2	0	2	0	8	.	4
4	2	0	2	1	0	.	5
4	2	0	2	1	6	.	5
4	2	0	2	1	8	.	6
4	2	0	2	9	9	.	4
5	2	0	2	9	9	.	4

Furthermore a table with specific information about each single case was generated and analyzed. Following properties have been documented (if known) in addition to the AIS code: year, gender, age, seat belt, airbag activation, vehicle type, seat position, accident type, collision velocity, height, weight, died on scene, died in hospital. For several cases documents with additional information about the injuries were available and looked through as well.

The review of statistical data of Statistik Austria was necessary to make a comparison between this data and those of CEDATU. The data of people died due to specific injuries are classified according to the international classification of diseases short ICD10-Version13. According to ICD10 traumatic rupture of the aorta was classified as S25.0, which is found in chapter XIX injuries, toxicities and certain other conse-

quences of exterior causes, S25 injuries of thoracic blood vessels. Furthermore the annual report of killed persons in traffic accidents of Statistik Austria has been observed.

The statistical parameter *odds ratio* is used for comparing risk of suffering TRA in a lethal accident. The following figure shows the table for calculation of the relative risk (RR) as well as the odds ratio (OR).

		Outcome			total	risk	
		+	-				
Exposure	+	a	b	a+b	$a/(a+b)$	$RR = \frac{a/a+b}{c/c+d}$	
	-	c	d	c+d	$c/(c+d)$		
total		a+c	b+d	N			
odds		a/b	c/d				
		$OR = \frac{ad}{bc}$					

Figure 2.1: Calculation of relative risk (RR) and odds ratio (OR)

2.3 Uni-axial extension test

Weisbecker et al (2012) presented the experimental data from uniaxial tension tests of human thoracic and abdominal aortas. The authors proposed a constitutive material model later in Weisbecker et al. (2015). The fitting of the parameters was done against the thoracic specimen of donor XI. Consistently the Freed-Einstein model in this study was fitted against the experimental data obtained with the specimen from donor XI.

2.3.1 Matlab Model of Freed-Einstein Constitutive Model

In another attempt the material model *MAT_266 (or *MAT_TISSUE_DISPERSSED) of LS-Dyna were implemented in the program Matlab. The definition of material parameters was approximated with the 'Freed-Einstein' model:

$$\mathbf{S} = \kappa J(J-1)\mathbf{C}^{-1} + \mu J^{-\frac{2}{3}} \mathbf{DEV} \left[\frac{1}{4} (\mathbf{I} - \bar{\mathbf{C}}^{-2}) \right] + J^{-\frac{2}{3}} \sum_{i=1}^n [\sigma_i(\lambda_i) + \varepsilon_i(\lambda_i)] \mathbf{DEV}[\mathbf{K}_i]$$

The default setting was following:

- Standard Neo-Hook model: $NHMOD = 1$
- Fiber dispersion parameter: $F = 1$
- Passive crimped fiber model is used: $FID = 1$

The above mentioned equation was calculated in several functions in Matlab and the single terms were explained in the previous chapter modeling of arteries – Freed-Einstein model. Here is shown a short overview of the functions.

Table 2.2: Structure of Matlab-source code for calculating the 'Freed-Einstein' model

Main Program	
	Definition and Selection of data
	Input of material parameters
	Calculation of data
	<i>Function Mat266ParameterCalculation</i>
	Plotting the output

Function Mat266ParameterCalculation	
Input: <i>F, SIGMA, MU, NY, FID, ORTH, C1, C2, C3, THETA, NHMOD, XX, YX, ZX, XV, YV, ZV, BETA, F_defgrad</i>	Output: <i>2nd PK-Stress-Tensor (PK2), Cauchy stress (SIG) and 1st PK-Stress-Tensor(PK1)</i>
Calculation of Jacobian matrix of the deformation gradient	
Calculation of the right Cauchy-Green deformation tensor	
Calculation of isochoric part of the Cauchy-Green deformation tensor	
Calculation of the hydrostatic term and isotropic deviatoric term	
Calculation of the anisotropic deviatoric term	
	<i>Function Dispersion</i>
	<i>Function PassiveFibre</i>
Calculation of the total stress tensor (2 nd Piola-Kirchhoff)	
Conversion to Cauchy stress	
Conversion to nominal stress (1 st Piola-Kirchhoff)	
Function Dispersion	
Input: <i>xXX, xYX, xZX, xXV, xYV, xZV, xt, xF, xSIGMA</i>	Output: <i>dispersion tensor (K)</i>
Calculation of Q	
	<i>Function Trafo</i>
Calculation of K	
Function PassiveFibre	
Input: <i>FID, C1, C2, C3, lmbd</i>	Output: <i>nominal Stress (Sgm_e), 2nd PK-Stress-Tensor (S)</i>
Calculation with crimped fiber model	
Calculation with exponential fiber model	
Conversion to 2 nd Piola Kirchhoff stress	

Function Trafo	
	Input: $x_{XX}, x_{YX}, x_{ZX}, x_{XV}, x_{YV}, x_{ZV}, xt$ Output: transformation tensor (Q)
	Defining the vectors for transformation
	Calculation of the unit vectors
	Forming of transformation-tensors R and T
	Combining the two transformation-tensors to get Q

The parameters of the Freed-Einstein model used in Matlab are shown in the following table with a short explanation.

Table 2.3: Short explanation of parameters used in Matlab for Freed-Einstein material of LS-Dyna

Parameter	Explanation
F	Fiber dispersion parameter
Sigma	Extent of dispersion
Mu	Shear modulus of elastin [GPa]
Ny	Poisson value
FID	Fiber model; crimped (1) or exponential (2)
ORTH	Number of fiber families
C1	Amplitude of fibers normalized to radius of fiber
C2	Wavelength of fibers normalized to radius of fiber
C3	Elastic modulus of the collagen fiber [GPa]
THETA	Angle between mean fiber direction and fiber families [°]
NHMOD	Type of Neo-Hookean model
BETA	Material angle (rotation about z-axis) [°]

2.3.2 LS-Dyna Single Element Model

Additionally material parameters were fitted by employing a single element model in LS-Dyna. The below mentioned formula was used to fit discretized data from biomechanical experiments. In the first part of the fitting process these results were further used as function parameters for the exponential 'Freed-Einstein' model. (Freed et al., 2005)

$\sigma_e(\lambda) = C_1 \lambda^{-1} \left(e^{\frac{C_2(\lambda^2-1)}{2}} - 1 \right)$	Formula 2-1: Calculation of stress (Sigma) with known stretch (Lambda)
--	---

This first part of parameter fitting was realized in Matlab and included a manual optimization. The parameters C1 and C2 are necessary to define a reference fitting curve for the second part of the parameter fitting process.

The second part was realized in HyperStudy, which is a software to perform Design of Experiments (DOE), approximations, optimization and stochastic studies. It is a convenient software package to study different aspects of a design under various conditions, including non-linear behavior. HyperStudy is part of the HyperWorks suite. DOE Studies are conducted in three steps: (1) Design space sampling, (2) Run DOE and (3) Evaluate results. After a successful DOE run further optimizations can be made. In either case design variable are defined together with a user-specified upper and lower threshold values. Further an objective of optimization has to be defined, against which the results are evaluated. (Altair HyperWorks, 2016)

With HyperStudy it was possible to use the LSDyna-model and to perform optimization automatically, with varied threshold values for the different layers. The parameters got fitted independently for each layer with the objective to minimize the least-squares between reference and model curve in circumferential and axial directions.

2.4 Inflation test

The inflation test simulates the material behavior of a three-layered aortic segment with the before fitted parameter and makes it possible to compare them with experimental data result. The experimental data for this test are only available for common carotid arteries (CCA) and internal carotid arteries (ICA). (Sommer and Holzappel, 2012) Thus a qualitative comparison is made as it is assumed that this material behavior is similar to that one of the thoracic aorta.

The thicknesses of intima, media and adventitia layer were taken from a biomechanical study of the thoracic aorta and were 0.48 mm, 1.18 mm and 0.93 mm, respectively. (Weisbecker et al., 2012)

Following assumptions are made:

$$l_u \sim 1 \text{ (So that } n_u \text{ is whole-numbered)}$$

$$l_e = 1$$

Thus:

$$l_u = r_i \frac{2\pi}{n_u} \quad \Longrightarrow \quad n_o = (2\pi r_i)_{\text{round}}$$
$$\quad \Longrightarrow \quad \gamma = \arccos \left(1 - \frac{\pi}{n_u} \right)$$
$$\quad \left(\gamma = \arccos \left(1 - \frac{l_u}{2r_i} \right) \right)$$

The following figures show drafts of one element consisting of three layers, the degrees of freedom and the node IDs.

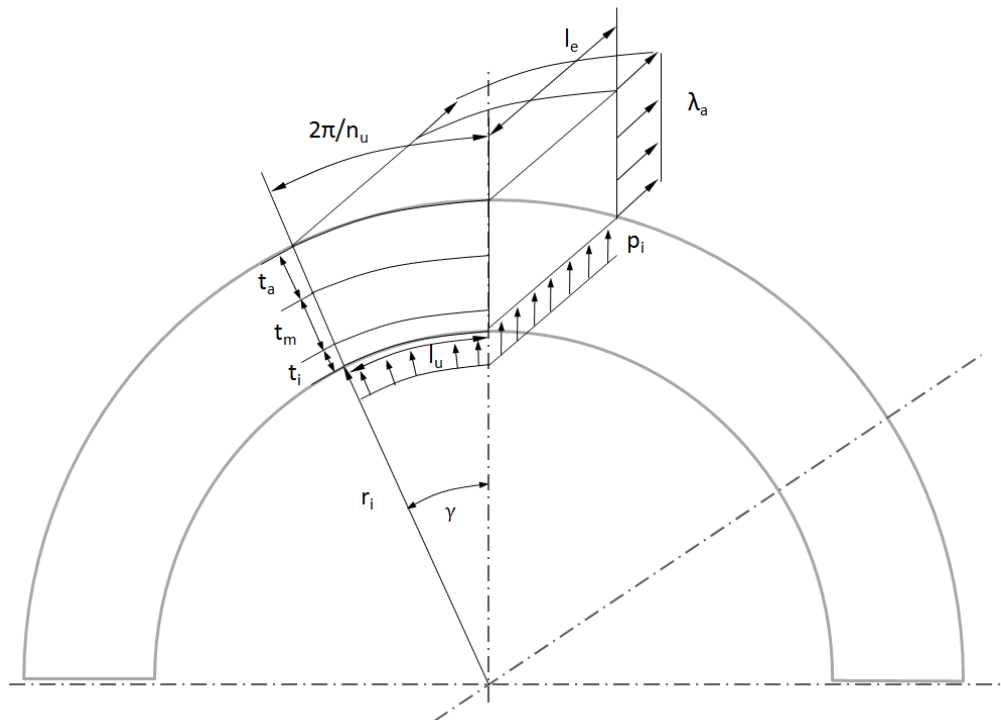


Figure 2.2: Draft of inflation test element

(t: thickness, a: adventitia, m: media, i: intima, ri: inner radius, pi: internal pressure, le: length of element, lu: inner segment length, nu: outer segment length, λa: axial strain)

DOFs

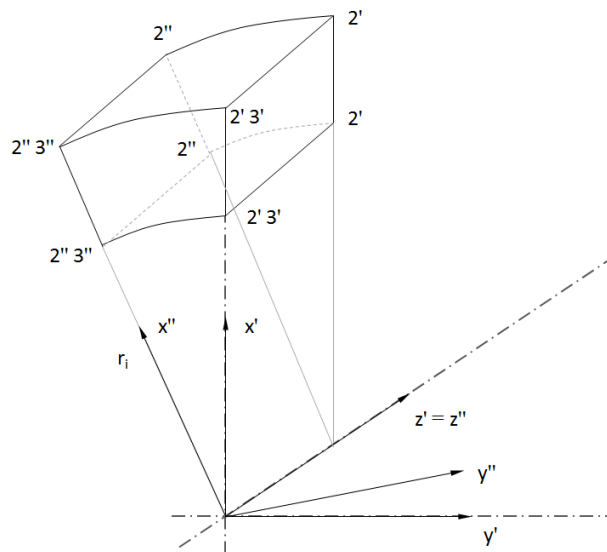


Figure 2.3: Draft of the degrees of freedom

(2: constrained in y direction, 3: constrained in z direction). Apostrophes refer to the referenced local coordinate system

NODE IDs

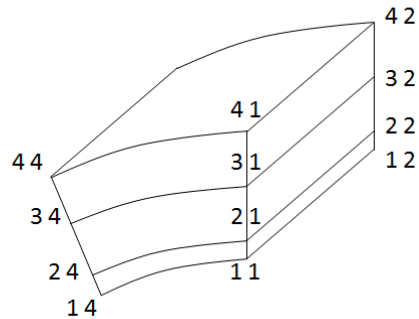


Figure 2.4: Draft of the node IDs for the different layers

For the inflation test have been defined parameters (INILMDZ, T2 and T3) and Sensors (SID1, SID2 and SID3). These were necessary for different expressions (see the next table).

Table 2.4: Parameters, sensors and expressions used for inflation test with a short explanation

Parameters	INILMDZ	initial axial pre-stretch
	T2	time after letting vessel equilibrate (load free)
	T3	time after pre-stretching vessel in axial direction
Sensors	SID1	Sensor Define Misc, Time: Calculation time
	SID2	Sensor Define Node, Coord: Node z-coordinate N201 (= axial length)
	SID3	Sensor Define Force, X-Section: Fz (=axial force)
Expressions	INILZ=SID2(T2)	measure length at time T2
	INIDZ=INILZ*(INILMDZ-1)	calculate z-displacement
		displace N201 by INIDZ
	FZ=SID3(T3)	measure z-cross-section force at time T3
		apply z-force at N201

The inflation test consists of 5 time steps.

- The first phase is the 'initialization' of the residual stretches of the two layers intima+media and the adventitia (it is assumed that intima and media have the same residual stretches). At the beginning of this phase a boundary conditions (BC) is activated, constraining the relative z-displacement of the nodes at the upper end of the element (Constrained Node Set). (In that way the upper end of the media+intima elements remains 'flat'). At the end of this phase the pre-scribed final geometry gets deactivated. At the same time the two layers (IM and A) are tied.
- The second phase is 'equilibration', which is the time to equilibrate the residual stretches. During this phase global damping is turned on to gain equilibrium without explicit-implicit switching. At the beginning of this phase layers are tied, single point constraints (SPC) at the edges are applied and the 'vessel cap' is connected to the upper end of the vessel through a 'Tie Break' contact. At the end of this phase the z-coordinate of Node 201 is measured, which is the initial length of the load free vessel.
Remarks: The SPCs assigned to the edges of the vessel establish a symmetry boundary condition. The vessel cap has no mechanical properties. I.e. the cap is assigned a 'null' material. The cap is required in the fourth phase, where the intraluminal pressure is build up. The cap imposes no forces in circumferential or radial direction. Due to a constrained node set, though, constraining the movement of the cap's nodes in z-direction (axial direction), the cap can transfer loads in axial direction. In summary, the cap transfers the axial loads due to the intraluminal pressure and additionally the axial force due to the axial pre-stretch.
- In the third phase the axial pre-stretch is initialized. In this phase the axial pre-stretch is prescribed as function of the initial load free length (i.e. the z-coordinate of Node 201 determined at the end of phase 2). The prescribed motion in axial direction is activated at the beginning of the third phase and deactivated at the end. At the end of the third phase is the axial force F_z to gain the required axial pre-stretch.
- In the fourth phase the intraluminal pressure is build up. First, the axial pre-stretch is switched from displacement-driven to force-driven, i.e. the force F_z determined at the end of phase 3 is loading the cap's centre and kept constant for the remainder of the simulation time. Additionally the inner wall (intima) as well as the cap is loaded by a pressure load. The pressure linearly ramps up till the end of phase 4.

- In phase 5 the equilibrium is established. To dampen out any nodal velocities that have been built up in phase 4, global damping is turned on. This last phase is the time to let the system equilibrate. The results are saved during simulation process and can be shown with the d3plot-file in the program HyperView.

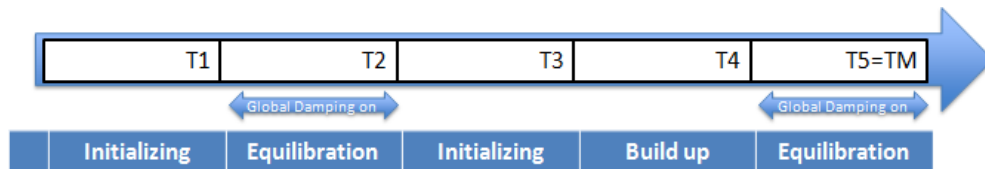


Figure 2.5: Overview of time steps for the inflation test

A second attempt was to execute the inflation test with equal residual stretches to check whether there is an influence or not.

2.5 Impact test

The simulation for the impact test is realized with a three-layered wall (intima, media and adventitia) cylindrical tube filled with fluid and closed with two tabs at its ends. A cylindrical impactor is positioned in the middle of the vessel. The impactor has a mass of 1kg, and an initial vertical velocity of 2.0m/s. The entire model is exposed to gravitational loading. The simulated impact duration is 30ms, 50ms and 100ms, respectively. Two models were compared: Model A is using the three-layered solid aortic wall employing the Freed-Einstein material model. Model B is using the one-layered shell aortic wall employing the fabric material model as used for example in the GHBM. Material parameters of model A were established in this study. Material parameters of model B were adopted from the GHBM model. The fluid and fluid-structure-interaction model as established in the preceding master thesis by Artner, 2016 was employed in Model A.

Dimensions of the straight tube section were selected such to be representative for the ascending aorta of an average adult male: 30mm outer diameter, 300mm in length, wall thickness (intima, media and adventitia): 0.48, 1.18 and 0.98mm.

The components of impact test of model A are shown in Figure 2.6.

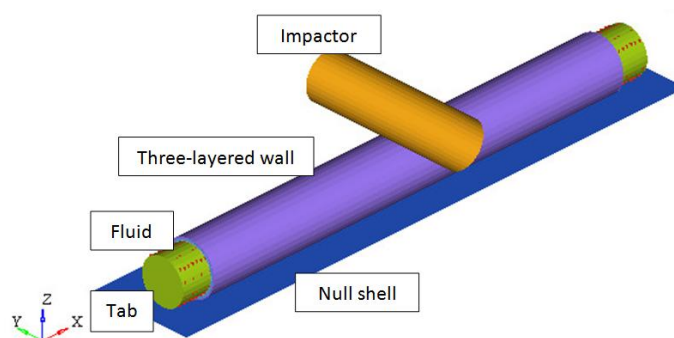


Figure 2.6: Components of impact test simulation

2.6 Full body impact

For the full body impact simulation with the human body models first of all the vehicle interior has been modeled.

The following elements were defined:

Seat cover

- deformable thin fabric cover
- 2D shell elements, which enclose volumes

Seat foam

- impression of seat bench according to weight of the dummy child
- 3D tetramesh, element size 4-5mm
- material properties adopted from industrial-quality-graded vehicle model for occupant simulation

Seat lower surface, tunnel and footwell

- 2D shell elements, mostly quads
- rigid material

At the moment CHARM-10 is the only available human body model of a 10 year old child that can be used for impact simulations. Prior to the impact simulation, pre-simulations were required for establishing the equilibrium and for positioning the seat belt.

The model was converted to the unit-system mm, kg, ms, kN, GPa. In the first pre-simulation, the human body model was exposed to the gravitational load, until the contact force equaled the weight of the occupant. In that way neither artificial damping, nor implicit-explicit code switching is necessary, to gain an equilibrium. In

the main impact simulation, all nodal velocities of the pre-simulation are zeroed, while keeping the internal energies (i.e. stresses in the seat foam and the buttock).

In the present case the simulation was not restarted, but the nodal coordinates from the pre-simulation were simply copied to the input deck. The initial internal energies and initial strains in the seat foam and the buttock flesh are simply calculated internally by the FEM solver then – by considering the initial nodal coordinates and the nodal coordinates calculated in the pre-simulation.

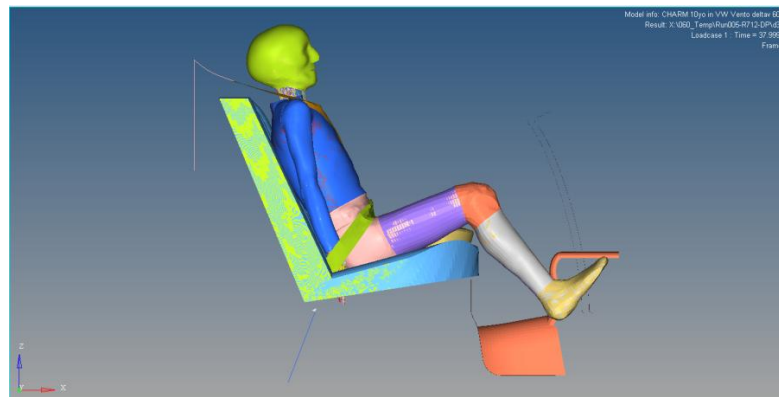


Figure 2.7: Seated CHARM at time step 37.99ms with a contact force of 0.346kN

The next step was the extraction of the node coordinate information and the creation of several include files. The node coordinates got saved into seven files (file-name in parentheses):

File 1: all node coordinates of CHARM model in undeformed condition
(001_CHARM_undeformiert.inc)

File 2: all node coordinates of rump part in undeformed condition as Initial_Foam_Reference (002_Sitzfleisch_undeformiert.inc)

File 3: all node coordinates of BiW model in undeformed condition
(003_BiW_undeformiert.inc)

File 4: all node coordinates of seat foam in undeformed condition as Initial_Foam_Reference (004_Sitzschaum_undeformiert.inc)

File 5: all node coordinates of seat foam and cover in deformed condition
(005_Sitzschaum_Bezug_deformiert.inc)

File 6: all node coordinates of complete CHARM model in deformed condition
(006_CHARMgesamt_deformiert.inc)

File 7: all node coordinates of car floor parts, booster, seat surface, driver seat and front passenger seat as well as the belt in undeformed condition
(007_Fussraum_Gurt_undeformiert.inc)

3 Results

3.1 Accident Analysis

The accident analysis of cases in the CEDATU showed that all in all 30 persons are documented in the years from 2003 to 2009. These cases can be split into 2 motorcyclists, 10 pedestrians and 18 passenger car occupants. The following sub items show a detailed overview of the results.

3.1.1 CEDATU-cases with TRA

Table 3.1 shows the number of persons with TRA, divided into accidents with pedestrians and accidents with occupants, compared to all in an accident injured of CEDATU.

Table 3.1: Registered cases in CEDATU with TRA-injury

Year	pedestrians			occupants		
	all injured	all lethal injured	TRA	all injured	all lethal injured	TRA
2003	76	75	8	434	168	8
2005	45	39	1	182	65	1
2006	-	-	-	180	61	1
2007	39	35	1	300	129	2
2008	34	-	-	227	93	3
2009	-	-	-	18	4	3

3.1.2 Occupant/pedestrian common overview

Considering all TRA-cases, about one third are female and two thirds were male. The mean age of females was 61.9 ± 24.0 years; the mean age of males was 45.5 ± 21.7 years. Death on scene occurred in 64% of all cases and 33% died in hospital, only 3% survived TRA.

Considering only car occupants, it was shown that 72% used a seat belt and 28% did not. In 50% of these cases the victim was the driver, in 33% it was a front-seat passenger and in 17% it was a rear-seat passenger.

Aortic rupture survival

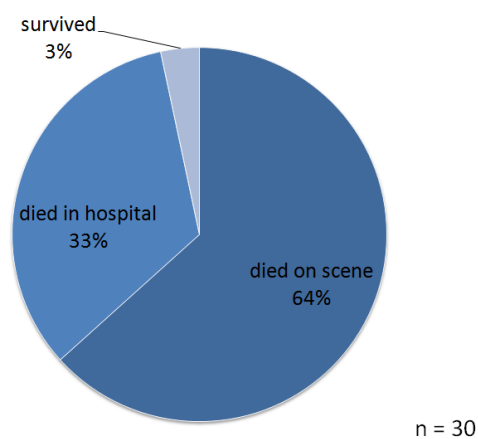


Figure 3.1: Percentage of aortic rupture survival of analyzed CEDATU cases

3.1.3 Occupant/Pedestrian: age groups

An analysis of the age of occupants and pedestrians showed that 3 occupants were between 5 and 14 years, and older than 65 years, respectively. One person was between 14 and 25 years and two persons were between 25 and 45 years. The biggest group was 'occupants between 45 and 65 years'; with a number of 9. Considering pedestrians the result turned out similar. The biggest group of injured pedestrians was aged between 45 and 65 years and showed a quantity of 5; followed by 3 injured who were older than 65 years. Between 14 and 25 years and between 25 and 45 years occurred one injury in each case.

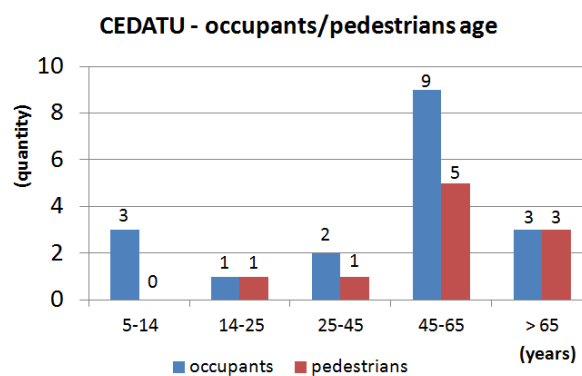


Figure 3.2: Age groups of occupants/pedestrians with TRA

The calculation of the Odds-Ratio (OR) for this age group showed that occupants between 45 and 65 years have an OR of 3.7 and that pedestrians between 45 and 65 years have an OR of 2.8.

3.1.4 Occupants: time series

In 2003 more than one third of the 434 occupant injured in a traffic accident were lethal injured. TRA occurred in 5% of all lethal injured. During the following years the number of TRA injuries remained approximately constant and constituted only 1.5% of all lethal injured. In 2008 about 3% of the 93 lethal injured were due to TRA. In 2009 only 18 injured occupants were documented. From these accidents were 4 lethal and 3 of them due to TRA, which would be equivalent to a percentage of 75%.

CEDATU – occupants

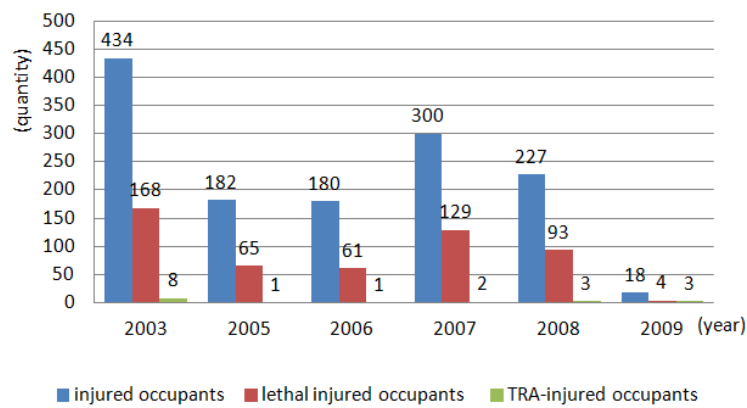


Figure 3.3: Time series of injured occupants, casualties and TRA cases

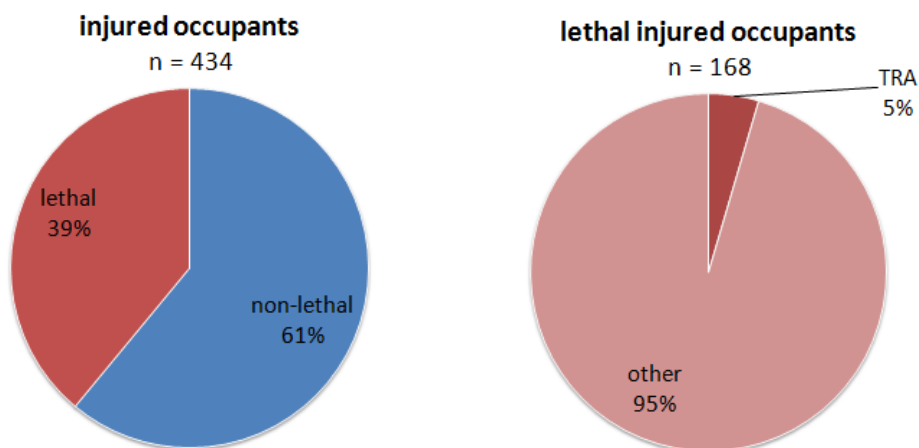


Figure 3.4: Percentage of TRA in occupants injured in traffic accidents of the year 2003

3.1.5 Pedestrians: time series

In 2003 more than 90 % of all injured pedestrians were lethal injured. TRA occurred in 11 % of all lethal injured pedestrians. In the years 2005 and 2007 the number of TRA injuries was approximately the same and constituted 3 % of all lethal injured pedestrians. In both years the number of lethal injured was between 86 % and 90 % of all documented injured pedestrians.

CEDATU – pedestrians

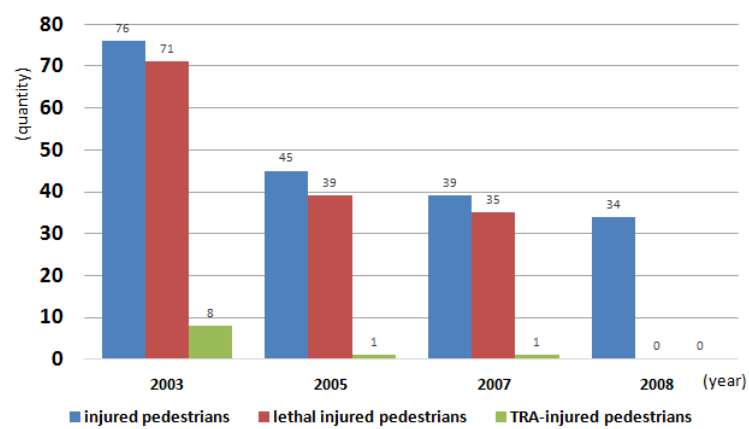


Figure 3.5: Time series of injured pedestrians, casualties and TRA cases

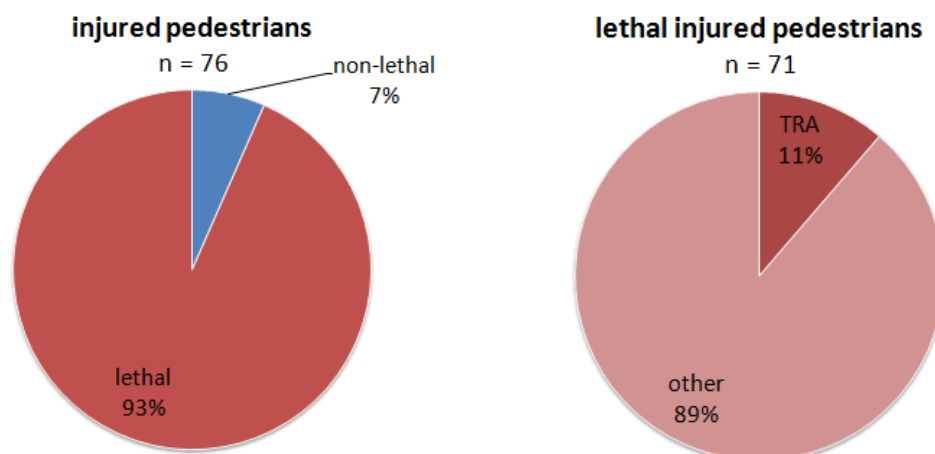


Figure 3.6: Percentage of TRA in pedestrians injured in traffic accidents of the year 2003

3.1.6 Location of TRA

The analysis of the observed cases showed that 3 aortic ruptures were located in the heart valve area and at the ascending aorta, 8 ruptured at the aortic arch and in the area of the fourth thoracic vertebral body, 7 were a rupture of the thoracic aorta and 2 were a rupture of the abdominal aorta.

The figure below summarizes the typical sites of TRA as found in the CEDATU cases.

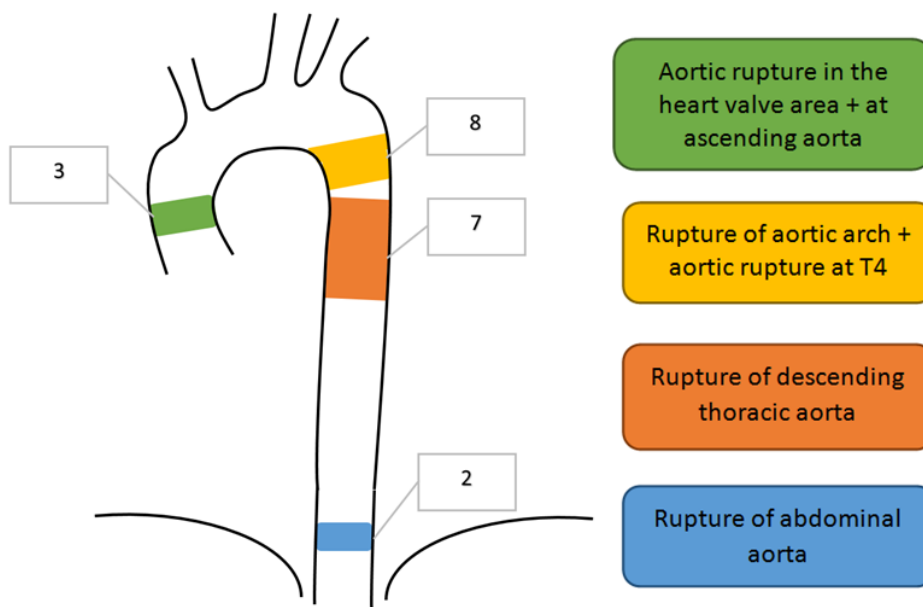


Figure 3.7: Location of TRA of analyzed CETADU-cases

3.1.7 Comparison CEDATU – Statistik Austria

The following table gives an overview of persons killed by TRA. The number of killed persons, registered in CEDATU, can be further segregated into 'died on scene' and 'died in hospital'.

Table 3.2: TRA-killed persons, Comparison Statistik Austria - CEDATU

Year	Killed persons (Cause of death: S25.0 Injury of the Aorta thoracica)	CEDATU (Injured persons with aortic rupture)	CEDATU - Died on scene	CEDATU - Died in hospital
2002	2	-	-	-
2003	-	16	11	5
2005	-	3	2	1
2006	-	1	-	1
2007	-	4	2	2
2008	3	3	2	-
2009	-	3	3	-
2011	2	-	-	-
2013	1	-	-	-

3.2 Uni-axial extension test

The following table shows the result from the first part, where the parameters for the exponential model got fitted to experimental data.

Table 3.3: Parameters for exponential model

Parameter	Intima	Media	Adventitia
C1 circ	0.02527	0.006264	0.009711
C2 circ	12.82	11.31	8.908
C1 ax	0.01556	0.0728	0.08184
C2 ax	12.06	2.515	6.479

The results of the second part are shown in the following table and figures. The table contains the values for each parameter for the particular layer with its minimum least-square configuration.

Table 3.4: Results from HyperStudy parameter fitting

Adventitia			LSQmin = 16.69
Theta	52°	Lambda	1.140
F	0.5	C1	0.70000000
Sigma	1.25	C2	8.03539081
Mu	7.689e-5 GPa	C3	0.0540000 GPa
Media			LSQmin = 35.16
Theta	40.1158°	Lambda	1.362
F	1	C1	0.29822929
Sigma	0.73307829	C2	2.02643608
Mu	3.73807e-5 GPa	C3	0.03198198 GPa
Intima			LSQmin = 4.07
Theta	44.023574°	Lambda	1.04643284
F	0.06431064	C1	0.70000000
Sigma	0.33298576	C2	7.66320000
Mu	1e-4 GPa	C3	0.03897241 GPa

In the following figures are shown the parameters for each layer with the minimum least-squares between reference and model curve in circumferential and axial directions.

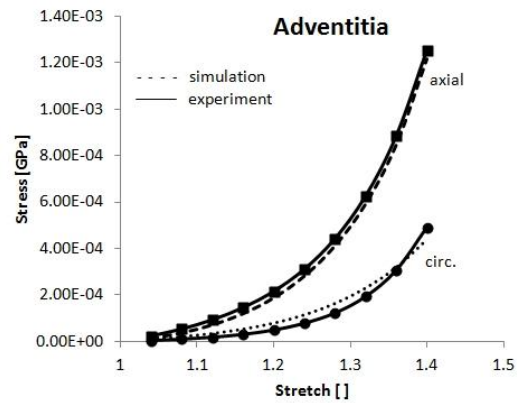


Figure 3.8: Reference and simulation curve for axial and circumferential stretch for the adventitia layer

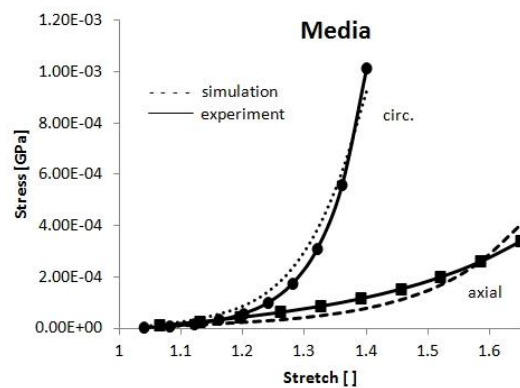


Figure 3.9: Reference and simulation curve for axial and circumferential stretch for the media layer

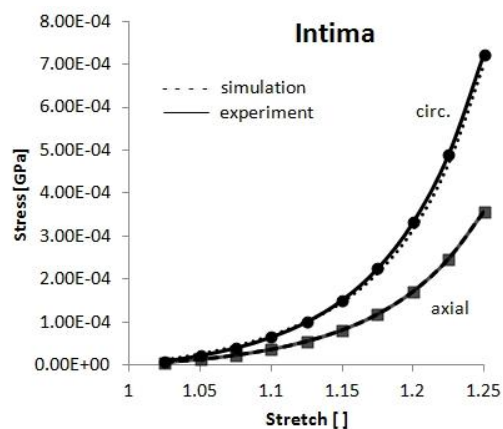


Figure 3.10: Reference and simulation curve for axial and circumferential stretch for the intima layer

3.3 Inflation test

The aortic segment for the inflation test is composed of several single elements, which got copied for result analyzing process. The pictures below show one element at time step 0 ms and time step 5 ms, as well as the composed aortic segment at the same time steps (for one selected axial pre-strain configuration). Further below are shown the results from the second attempt without residual stretches.

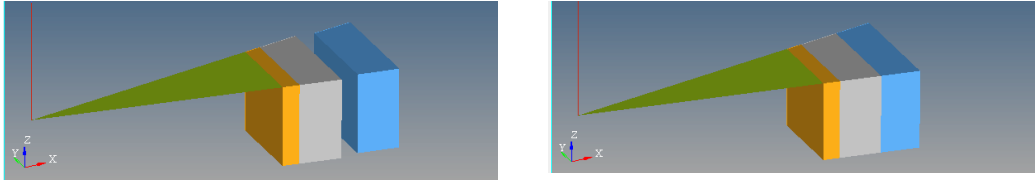


Figure 3.11: Single element for inflation test at 0ms (left) and 5ms (right).

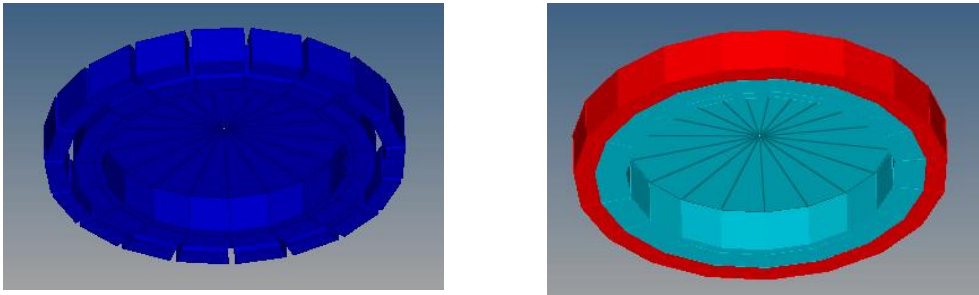


Figure 3.12: Circumferential strain of aortic segment at 0ms (left) and 5ms (right).
Maximum in adventitia layer: $5.827e-02$ GPa, media/intima layer: $1.714e-02$ GPa.

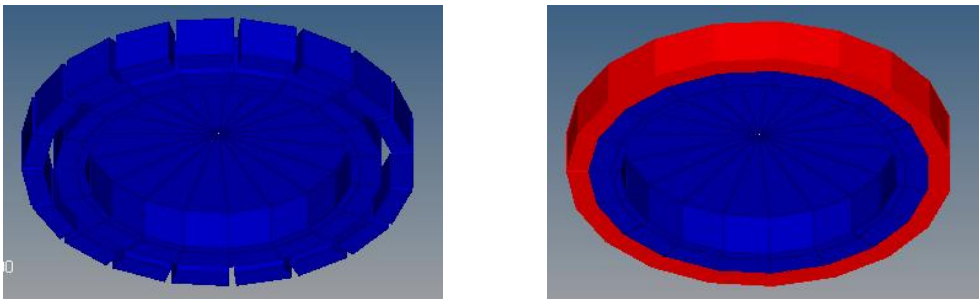


Figure 3.13: Axial strain of aortic segment at 0ms (left) and 5ms (right).
Maximum in adventitia layer: $1.210e-09$ GPa, Minimum in media/intima layer: $-6.803e-30$ GPa.

The following figure shows a plot of pressure and axial stretch at varied axial pre-strains of 0%, 5%, 10%, 15% and 20%.

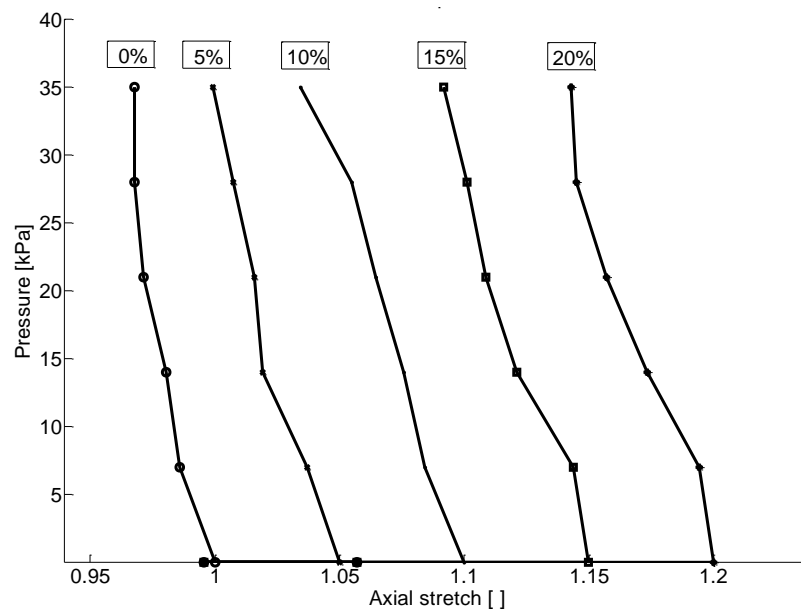


Figure 3.14: Pressure - Axial stretch curves for varied axial pre-strains (from 0% to 20%)

The next figure shows a plot of pressure and circumferential stretch at varied axial pre-strains of 0%, 5%, 10%, 15% and 20%.

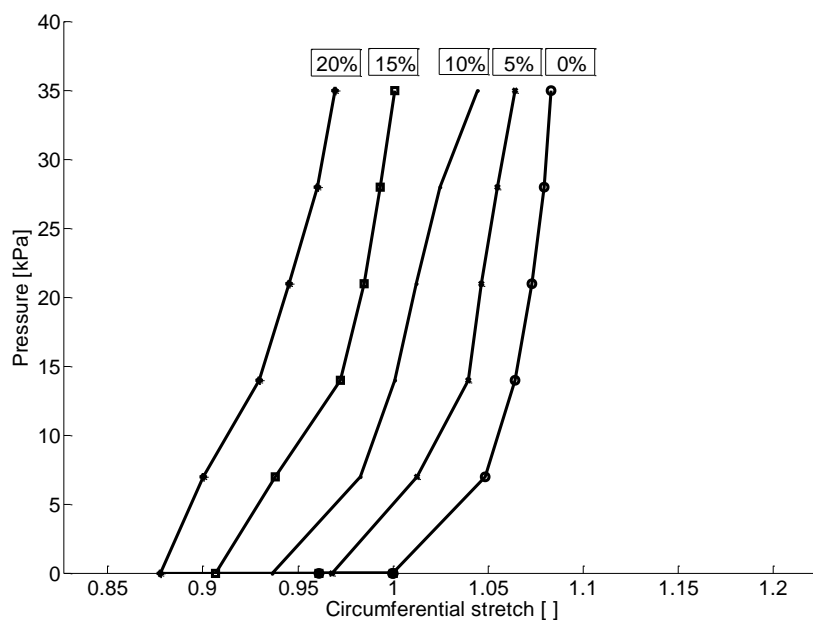


Figure 3.15: Pressure - Circumferential stretch curves for varied axial pre-strains (from 0% to 20%)

The following figures show a comparison between the single element, circumferential strain and axial strain of aortic segment once with consideration of residual stretches on the left side and once without consideration of residual stretches on the right side.

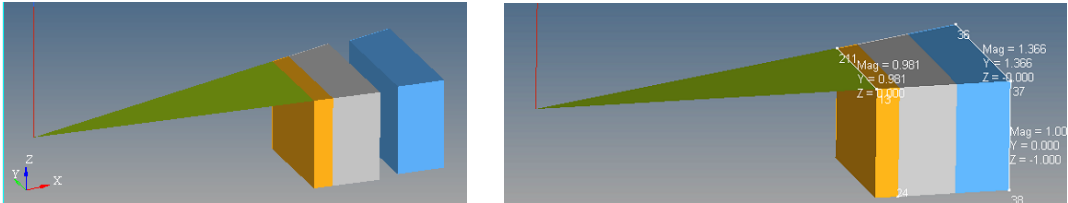


Figure 3.16: Single element for inflation test with (left) and without (right) residual stretches.

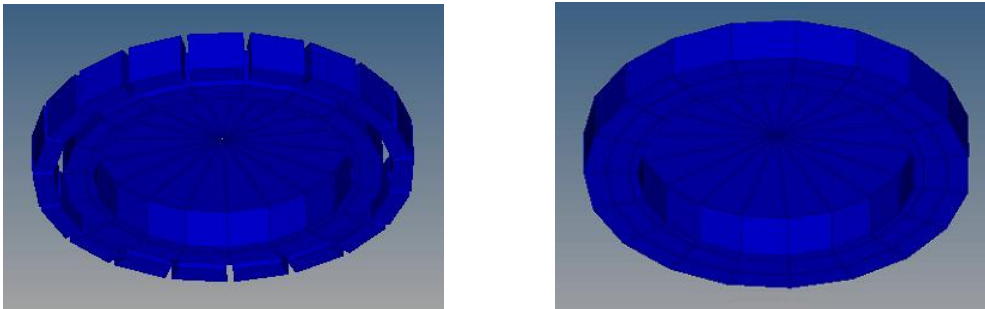


Figure 3.17: Circumferential strain of aortic segment with (left) and without (right) residual stretches.

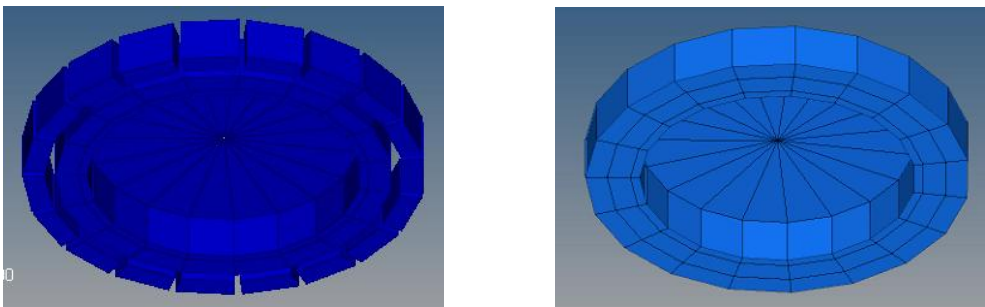


Figure 3.18: Axial strain of aortic segment with (left) and without (right) residual stretches.

The figure below shows a comparison of pressure and axial stretch curves at varied axial pre-strains of 0%, 5%, 10%, 15% and 20% in consideration of residual stretches.

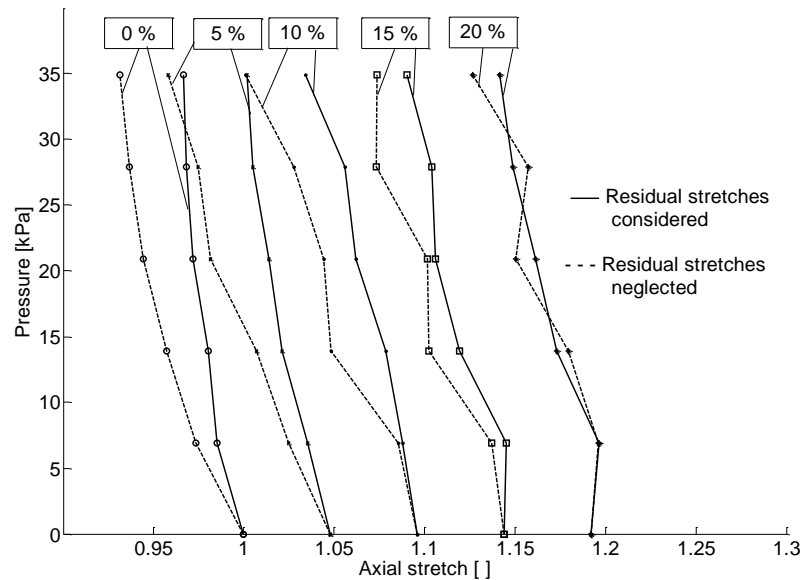


Figure 3.19: Pressure - Axial stretch curves for varied axial pre-strains (from 0% to 20%) with and without consideration of residual stretches

The next figure shows a comparison of pressure and circumferential stretch curves at varied axial pre-strains of 0%, 5%, 10%, 15% and 20% in consideration of residual stretches.

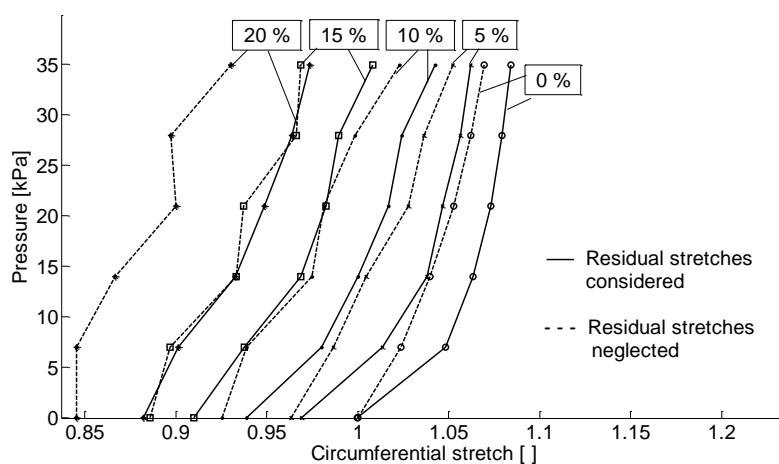


Figure 3.20: Pressure - Circumferential stretch curves for varied axial pre-strains (from 0% to 20%) with and without consideration of residual stretches

3.4 Impact test

The impact tests show obvious variation between model A, with Freed-Einstein parameters, and model B, with GHBMC parameters. The following figures compare displacement in z-direction, acceleration and energy of the impact test simulation (duration of 50ms) with model A and model B, respectively. Further below is shown the deformation at different time steps for each model.

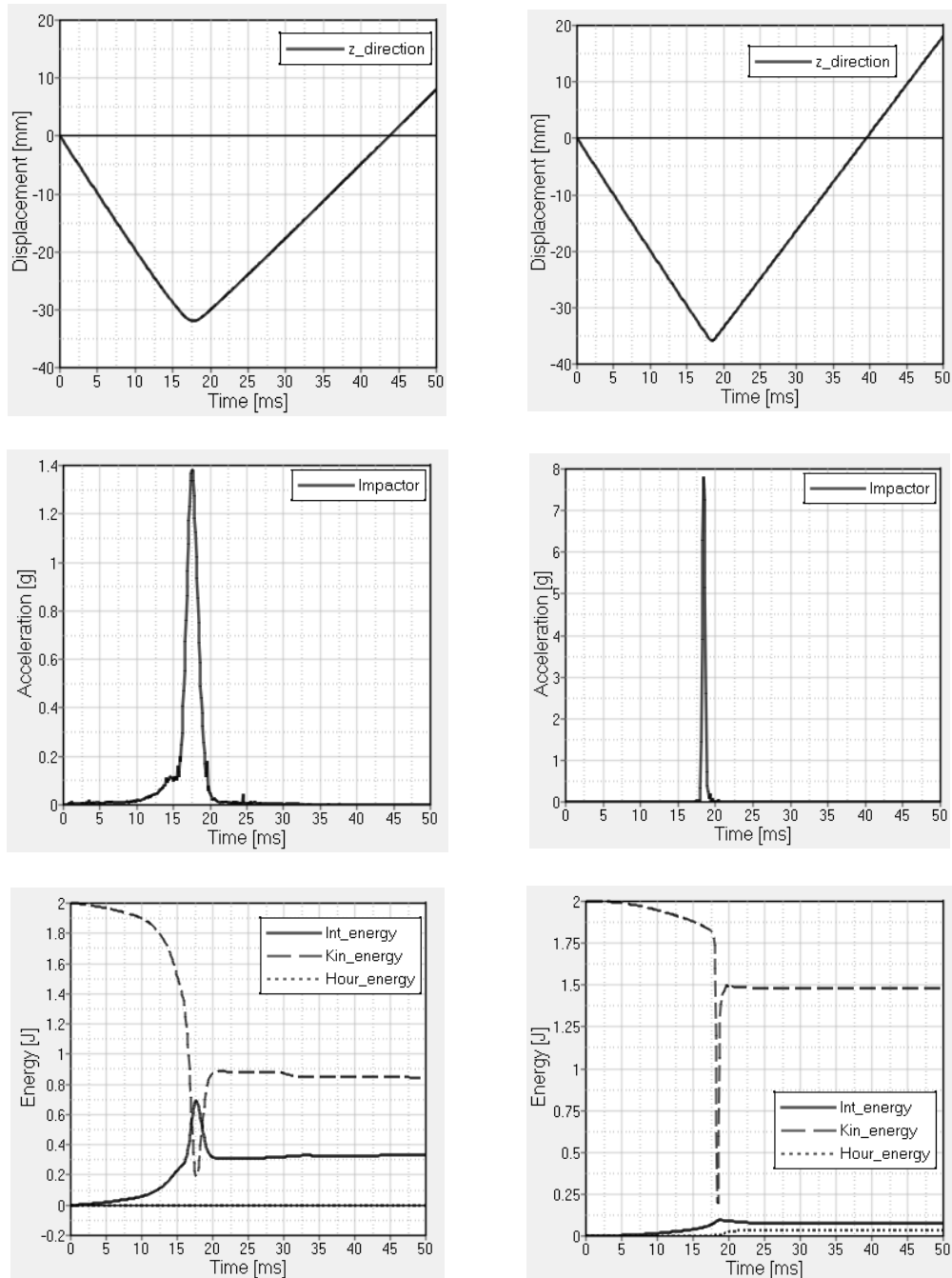


Figure 3.21: Displacement in z-direction, impactor acceleration and energy of impact test (left: model A, right: model B)

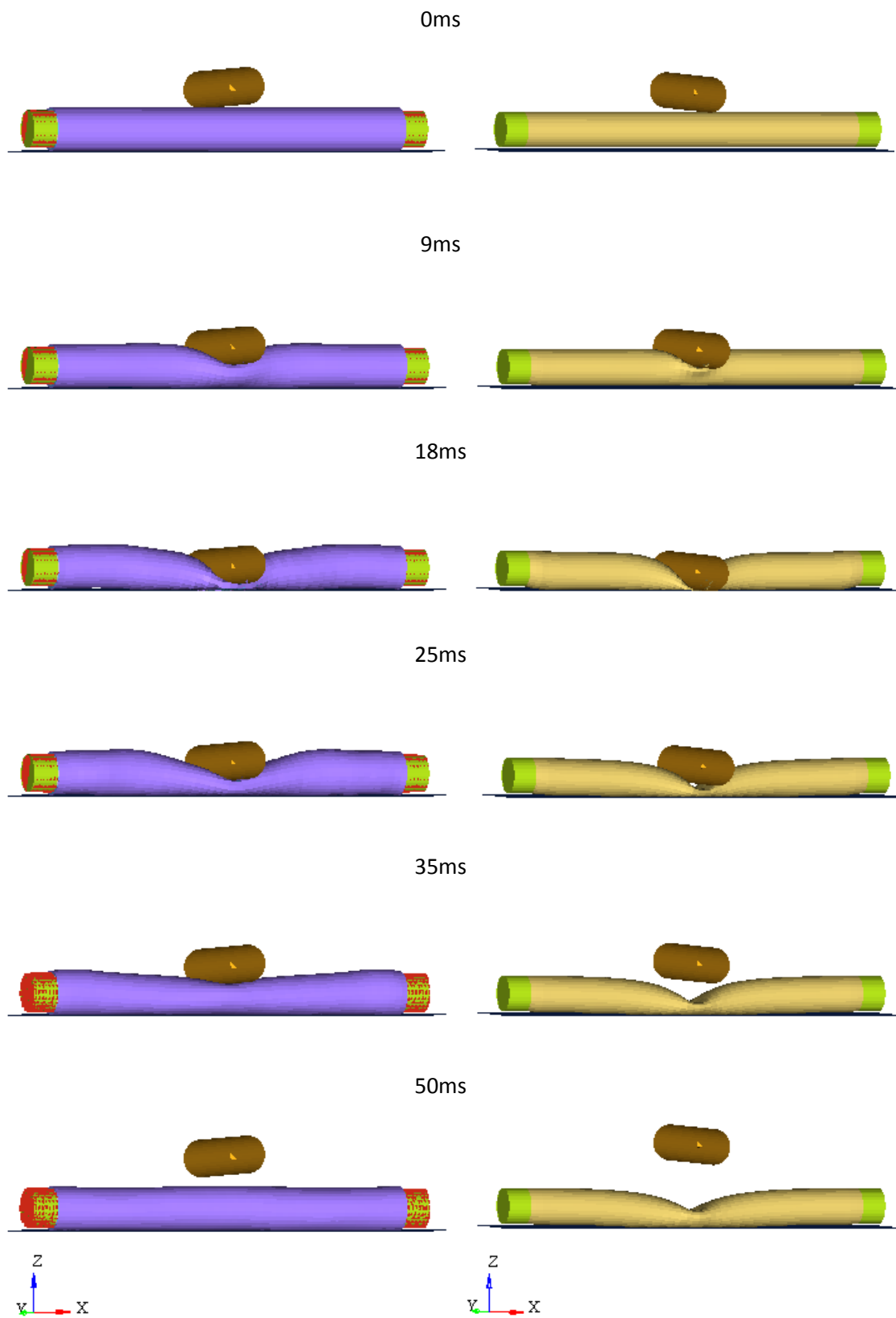


Figure 3.22: Deformation at different time steps for model A (left) and model B (right)

3.5 Full body impact

The pre-simulation with CHARM showed that it is not useful to further simulate with these results. First, the problem was that the seat belt penetrated into the thoracic flesh. The second problem was that the aorta-segments penetrated other body parts and third, the heart shifted to the left side. The following figures show these results of the simulation.

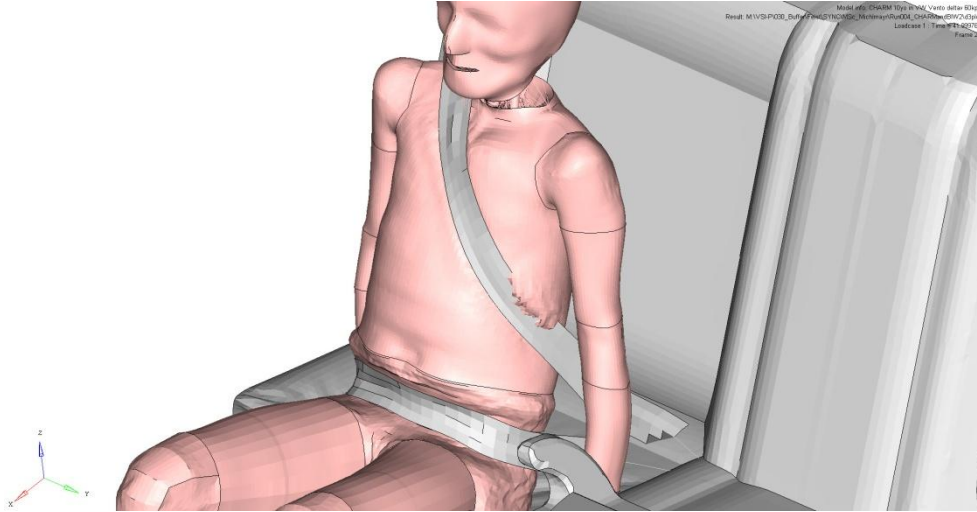


Figure 3.23: Result of pre-simulation - seat belt

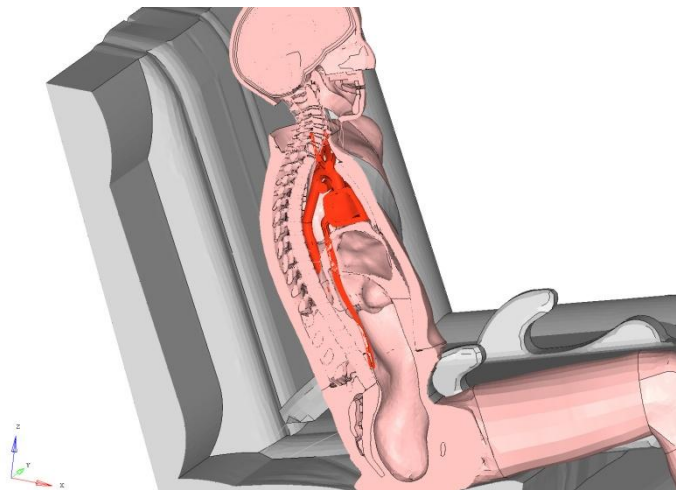


Figure 3.24: Result of pre-simulation - aorta segments

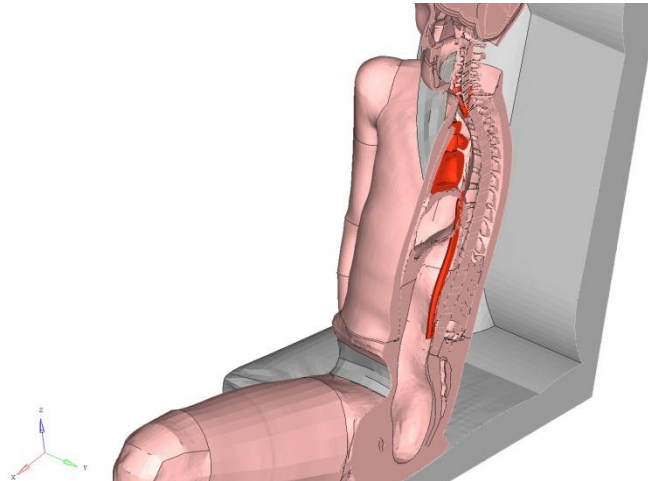
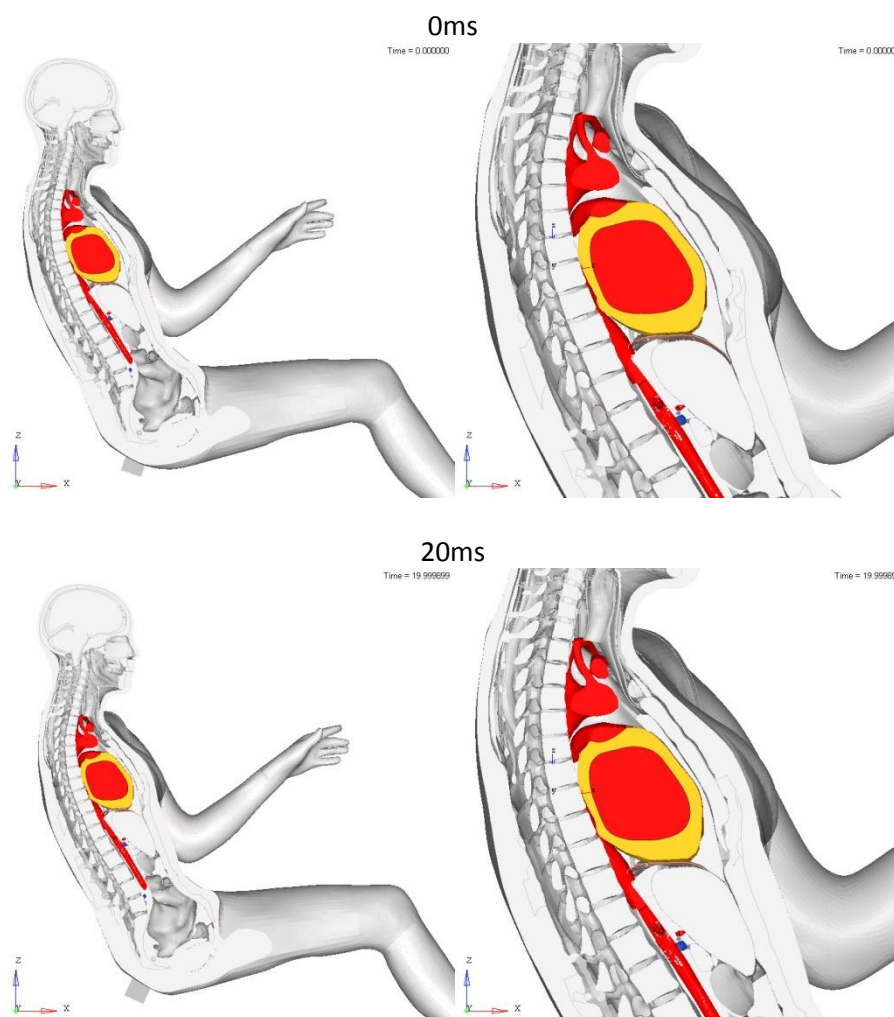


Figure 3.25: Result of pre-simulation - heart

The results of the full body impact simulation with the occupant model of GHBMC-F05 are shown in the figures below.



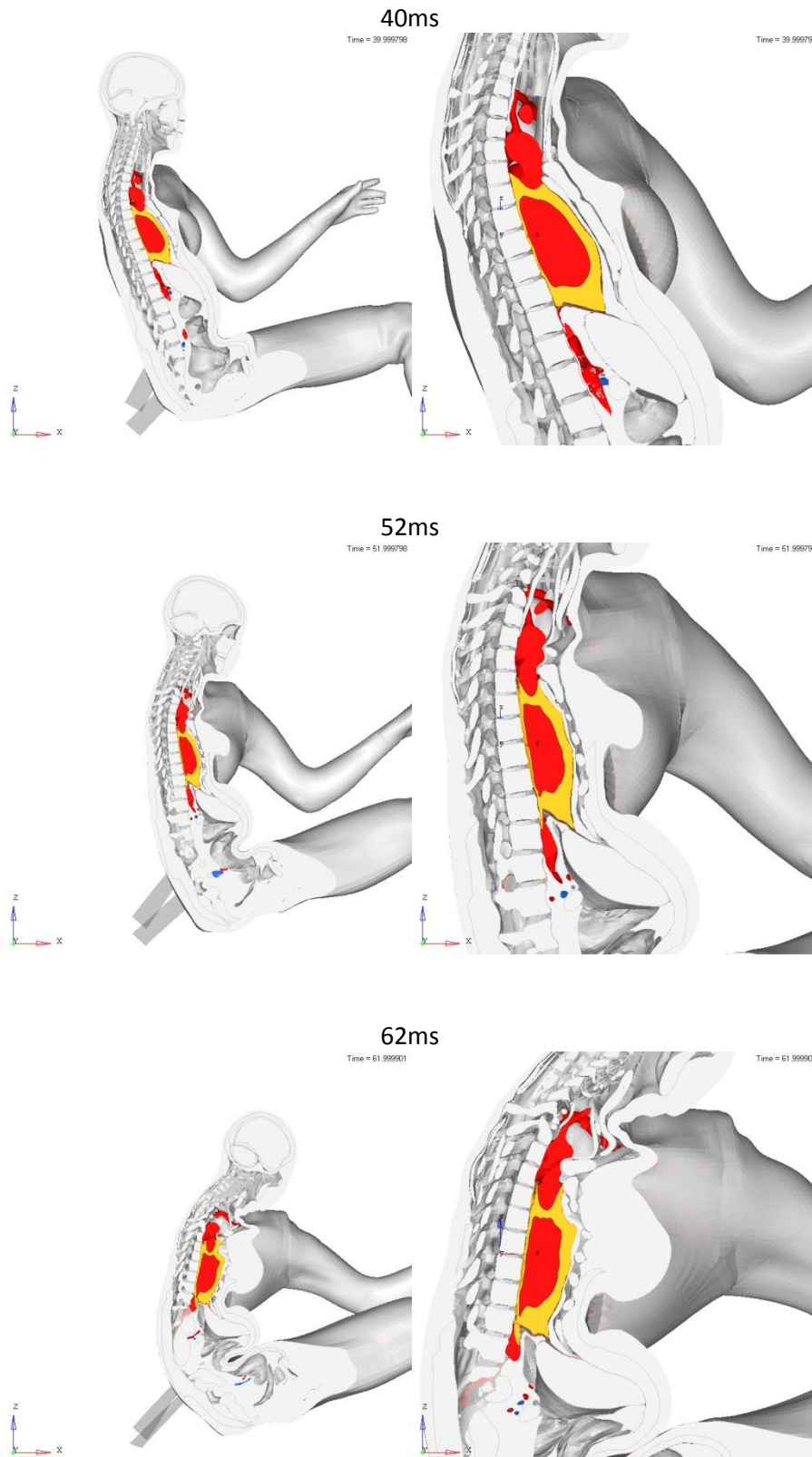


Figure 3.26: Simulation result with GHBM-C O F05 at different time steps

4 Discussion

4.1 Discussion of accident analysis results

In 2003 the number of documented accidents in the CEDATU was high. Therefore the year is an excellent candidate for a more thorough analysis.

The data of accidents of the year 2009 was not representative, as only 18 accidents were documented in CEDATU at the time of analysis. The calculated TRA-rate would have been 75%, as 3 of the 4 lethal accidents were due to TRA, and so no reliable scientific conclusion for this year can be drawn.

Blunt traumatic aortic rupture is a life threatening injury. In the UK it is responsible for more than 21% of all road fatalities and it has an overall survival rate of less than 2%. (Richens et al., 2003)

For the United States of America TRA rate is reported in approximately 16 – 35% of individuals who die after motor vehicle collisions. (Ryb et al., 2013)

The number of fatalities due to TRA in Austria is lower than in the UK or in the USA. The big difference here may arise in the manner of data acquisition. The signs and symptoms of TRA are non-specific and often there are additional distracting injuries present. This can result therein, that TRA is not the only or not the main injury which is documented. It is very likely that quite a large number of TRA cases in Austria are masked by assigning a 'polytrauma' – instead of further distinguishing injuries. Although the number of TRA cases in Austria is very low, the overall survival rate of 3% lies around that one of the UK. It has to be stressed that CEDATU was initiated as a database of lethal traffic accidents, so the low number of TRA cases in this analysis may be due to the fact that non-lethal accidents had only been documented recently.

A recent analysis of pedestrian accidents from Otte et al. (2016) shows that the differences of the accident situation nowadays and 40 years ago were leading to a reduction of TRA in traffic accidents. Some of the reasons for the reduction in aortic rupture in Germany over time are likely to be found in better car design and improved medical practices as well as better safety standards being implemented in vehicles. The improved pedestrian safety of new cars, pedestrian-friendly front structures of cars and automatic braking systems also contribute to reduce the number of severe injuries among pedestrians. (Otte et al., 2016)

The analysis of CEDATU cases with TRA showed that 90% of all ruptures are in the thoracic area of the aorta and 10% are in the abdominal area of the aorta. The thoracic area can be divided into aortic arch (40%), descending thoracic aorta (35%) and heart valve/ascending aorta (15%). So three quarter of all TRA cases are located at the aortic arch and the upper descending thoracic aorta. Compared to other studies this is a reasonable result:

- Most ruptures (68% of 37 road accident victims) affect the proximal descending aorta distal to the opening of the left subclavian artery, the isthmus. (Sevitt, 1977)
- Usual sites of rupture: the aortic isthmus just distal to the origin of the left subclavian artery, the ascending aorta, the lower descending thoracic aorta to the aortic hiatus to the diaphragm and the mid-arch portion. (Moar, 1985)
- The site of injury in 90% was the aortic isthmus, that is, distal to the origin of the left subclavian artery. In 8% the injury was in the distal thoracic aorta and 2% had injuries of the aortic arch. (Kodali et al., 1991)
- Autopsy data shows that aortic rupture is located as follows: 54 – 65% isthmus, 10 – 14% arch and ascending aorta, 8 – 12% distal descending aorta, 7 – 9% diaphragmatic or abdominal, 13 – 16% at multiple sites. (Burkhart et al., 2001)
- Computer simulation and cadaver studies showed that at the time of the crash, intra-aortic pressure increases. This pressure combined with rotational forces exerts the biggest stress at the isthmus. (Demetriades, 2012)

An analysis of the age of occupants and pedestrians showed that 3 occupants were between 5 and 14 years, and older than 65 years, respectively. The largest group of injured pedestrians was aged between 45 and 65 years and shows a quantity of 5. The calculation of the Odds-Ratio showed that older people have nearly a four times or three times higher risk of suffering a TRA in case of a traffic accident respectively. This result is consistent with a study which postulates that older adults have the highest rate of MVC related blunt thoracic aorta injury. (McGwin et al., 2002)

The accident scenarios were known in about two thirds of the registered CEDATU cases. From these 23 cases 65% were due to frontal impact and only 35% were due to side impact. Considering pedestrians accidents frontal impacts make the great majority. In the UK 29% were due to frontal impact and 44% were due to side impacts. (Richens et al., 2003)

Another study which postulates that the incidence of TRA in side impact (2.4%) was found to be twice as high as the TRA incidence in frontal impact (1.1%) shows accordance with the data of the UK. In general this study postulates that the risk of TRA increases with speed, intrusion into the passenger compartment, and subject age. (Hardy et al., 2008)

It seems to be hazy to define accident types which lead to TRA. A study about traumatic rupture conditions postulates that the combined effect of chest deceleration, chest compression and blood pressure appears to generate an aortic deformation and failure pattern that captures characteristics of clinically observed TRA. It reveals that a level of 280kPa pressure might cause TRA near the ascending aorta, but the 'usual' deformation pattern occurs in the above mentioned combined effects. (Lee and Kent, 2007)

A superficial analysis of data acquisition of STAT CUBE/Statistik Austria showed that data about TRA cases in traffic accidents needs to be considered with care as differences to other published traffic-accident-statistics of them may arise from following reasons:

- Complete coherence between cause-of-death-statistic and traffic-accident-statistic is not possible due to missing data of injured person and missing link to hospital information.
- Cause-of-death-statistics counts only fatally injured persons, who had their principal residence in Austria.
- Traffic-accident-statistics takes into account all fatally injured persons, who had an accident on Austrian state territory, independent if the person was an Austrian or not; so tourists and transients are included as well.
- Cause-of-death-statistics includes all fatally injured persons due to a traffic accident, independent of how long after the accident death occurs.
- Traffic-accident-statistics counts only injured persons dying within 30 days as a result of an accident.

4.2 Discussion of simulation results

The intention was to use already existing material models from LSDyna and to fit them to experimental data from biomechanical tests. This happened on different levels of aortic segments; from a single element to a quarter cylindrical part and a three-layered tube up to the whole descending thoracic aorta. Different approaches were applied to fit material parameters. The Matlab-model was developed for fitting material parameters based on uni-axial tests. Biaxial testing, though, was not considered or implemented yet.

The inflation test with the aortic segment provides satisfying results. So the pressure-circumferential stretch curves with different pre-strain levels are comparable to experimental data (Sommer and Holzapfel, 2012). However, pre-strains had not the same effect as was observed in the inflation tests for the CCA. Higher pre-strain levels lead to a curve-shift to lower circumferential stretches; inverted behavior at axial stretches. There higher axial pre-strain levels lead to axial stretch curves with

higher gradient. The accordance between model and experimental axial stretch curves in the lower pressure area is expandable. A comparison between simulation with and without consideration of residual stresses showed an obvious curve drift. This may indicate the importance of including residual strains as postulated in Holz-
apfel et al., 2000.

The impact test with the straight aortic segment showed that there is an obvious variation between model A and model B. The differences in the results are shown in displacement, acceleration of the impactor and deformation. The maximum displacement of model A (31.96mm) is smaller than that one of model B (35.92mm). The impactor acceleration of model B is five times higher than of model A, which may result from a completely compressed aortic segment and a contact between impactor and rigid wall element, i.e. bottoming out at 18ms.

Aortic injuries do not result from one specific mechanical factor. It is impossible to blame only the stretching of the aorta or shearing due to deceleration loads or only the increase of internal blood pressure as the main trigger for an injury. It is a combination of all these different mechanisms, which makes it difficult to limit this to one injury causing mechanism. Therefore a more thorough investigation by means of numerical simulation may help to pinpoint injury causation:

Occupant simulations with the human body model CHARM showed that the thoracic aorta seemed to meet the anatomical requirement, but generally the model showed room for improvement: Seemingly the contact definitions were incomplete, resulting in a number of initial penetrations between parts or non resolvable penetrations during impact simulations. Other problems were a shift of the heart to the left side and that aorta segments penetrated other body parts of the thorax flesh. The model (including the test setup) was provided to the developer for resolving the issues. Unfortunately, the developers were unable to resolve these issues. The developers indicated that the model is applicable for less severe impacts only. Maybe these simulations can be repeated and advanced in the future with an updated CHARM model.

Therefore simulations were repeated with the human body model 'GHBMC' model which terminated normally and showing no issues with respect to stability. The results showed that the injury mechanism 'osseous pinch' may be a possible injury cause. The simulation shows a huge contusion of the aorta (and the heart) around the thorax together with shearing strain between sternum and thoracic spine. This is in line with the study of Hardy et al., 2008 who stated that the principal component of injury causation was the stretch of the aorta, which was generated by the deformation of the thorax. (Hardy et al., 2008)

A negative aspect of the GHBMC simulation is that it fails to comply with the anatomy of a child.

Especially at a young age the inner organs are more likely to be injured in a car accident, due to the not fully developed bone structures and different body proportions compared to adults, which is a particular challenge in model development. (Eisenach, 2014) Due to ethical challenges biomechanical validation data of children is lacking and so no specific material parameters for children are available.

The results of this thesis can be used to establish an enhanced model of the thoracic aorta for HBMs. The model should consist of a three layered wall modeled with solids instead of shell elements, Freed-Einstein material parameters instead of isotropic linear elastic material models filled with SPH fluid elements.

The approach of SPH fluid is consistent to the study of Shah et al., 2001, who stated that fluid elements are helpful to simulate pressure changes inside the aorta due to impact.

Forman et al., 2008, highlighted that only the intra-aortic fluid pressure, but also the extra-aortic pressure should be considered for analyses of TRA. This was not done within the current thesis, but should be investigated in future works. Anyway, the challenge for future approaches will remain the balance between the need of biomechanical accuracy and the necessary simplification for time efficient application of the models in the automotive industry.

5 Conclusion

The analysis of the accident database CEATU showed that TRA occurs in about 5% of all fatal accidents. In literature relative frequencies of up to 25% have been reported. TRA is associated with a high mortality rate – reaching 97%. Only one case in CEDATU was found where TRA was survived.

TRA in traffic accidents was observed in pedestrians and occupants and occurred most frequently in the age group 45 – 65 years with an odds ratio of 3.7 compared to other age groups.

It was found that most of the ruptures occurred in the thoracic aorta. Especially the area of the aortic arch (40%) and the descending thoracic aorta (35%) were identified as the most frequent locations of TRA.

Several theories on underlying TRA mechanisms are available in literature, e.g. Osseous Pinch, Voigt's Shoveling and Water Hammer-Effect. The reconstruction of a real world accident employing a state-of-the-art human body model showed a huge compression of the aorta (and the heart) around the thorax together with a pronounced traction between sternum and thoracic spine.

Reviewing the modeling approaches used for the aorta in contemporary human body models, though, showed deficiencies and room for improvements. The fluid is mostly modeled as airbag, which does not allow for analyzing the effects of shock-waves or inertial forces induced by the fluid. The aortic wall is mostly modeled as a one-layered shell, disregarding the three-layered architecture of the aorta. The Freed-Einstein material model was found to be the only material model available in LS-Dyna featuring the required material properties to model the aortic wall in a very biofidelic way. It was possible to fit the material parameters to biomechanical data of the human thoracic aorta for uni-axial tests. A good correlation ($R^2=0.99$) was achieved with the fitted material parameters. Simulation of inflation tests were performed and showed a realistic behavior when compared qualitatively to biomechanical test data of the common carotid artery.

A comparison of impact simulations with the enhanced aorta model (employing the Freed-Einstein material) and aorta models used in current state-of-the-art HBMs showed significant differences in terms of deformations. The maximum deflection of the state-of-the-art model was higher (31.96mm and 35.92mm) and less energy

was absorbed. A lower maximum force of the impactor was observed when the enhanced aorta model was impacted.

The thesis shows that the Freed Einstein material model (*MAT_TISSUE_DISPERSSED) is applicable for modeling the human thoracic aorta in LS-Dyna. It should be applied in future HBM models in LS-Dyna instead of the conventional linear isotropic material models (e.g. *MAT_ELASTIC) or simple anisotropic models (e.g. *MAT_FABRIC). Together with an improved fluid-structure interaction and an enhanced fluid model, based on a smoothed particle hydrodynamics, the model described in this thesis will improve the biofidelity of human body models employed in the area of vehicle safety.

6 List of figures

Figure 1.1: Heart with aorta in the human thorax (Gumpert, 2015)	4
Figure 1.2: Anatomy of the aorta (Rakesh Sharma, 2014)	4
Figure 1.3: Different layers of the aorta (Holzapfel, 2003)	5
Figure 1.4: Possible injuries of soft tissue of the thorax (Schmitt et al., 2010).....	6
Figure 1.5: Blood Flow into false lumen - aortic dissection (adopted from U.S. National Library of Medicine)	8
Figure 1.6: Putative forces acting on the aorta during blunt traumatic injury (Richens et al., 2002)	9
Figure 1.7: Line drawing of osseous pinch mechanism (Cohen et al., 1992)	10
Figure 1.8: Cross-sectional views of the thorax, showing forces causing aortic injury according to the theory of the 'shoveling' mechanism. (Tribble and Crosby, 1988)	11
Figure 1.9: Draft of the mean fiber direction with 2 fiber families and the fiber dispersion parameter F	25
Figure 2.1: Calculation of relative risk (RR) and odds ratio (OR)	29
Figure 2.2: Draft of inflation test element.....	35
Figure 2.3: Draft of the degrees of freedom.....	35
Figure 2.4: Draft of the node IDs for the different layers.....	36
Figure 2.5: Overview of time steps for the inflation test	38
Figure 2.6: Components of impact test simulation	39
Figure 2.7: Seated CHARM at time step 37.99ms with a contact force of 0.346kN..	41
Figure 3.1: Percentage of aortic rupture survival of analyzed CEDATU cases	44
Figure 3.2: Age groups of occupants/pedestrians with TRA	45
Figure 3.3: Time series of injured occupants, casualties and TRA cases	46
Figure 3.4: Percentage of TRA in occupants injured in traffic accidents of the year 2003	46
Figure 3.5: Time series of injured pedestrians, casualties and TRA cases.....	47
Figure 3.6: Percentage of TRA in pedestrians injured in traffic accidents of the year 2003	47
Figure 3.7: Location of TRA of analyzed CETADU-cases	48
Figure 3.8: Reference and simulation curve for axial and circumferential stretch for the adventitia layer	51
Figure 3.9: Reference and simulation curve for axial and circumferential stretch for the media layer	51

Figure 3.10: Reference and simulation curve for axial and circumferential stretch for the intima layer.....	51
Figure 3.11: Single element for inflation test at 0ms (left) and 5ms (right).....	52
Figure 3.12: Circumferential strain of aortic segment at 0ms (left) and 5ms (right).	52
Figure 3.13: Axial strain of aortic segment at 0ms (left) and 5ms (right).....	52
Figure 3.14: Pressure - Axial stretch curves for varied axial pre-strains (from 0% to 20%)	53
Figure 3.15: Pressure - Circumferential stretch curves for varied axial pre-strains (from 0% to 20%)	53
Figure 3.16: Single element for inflation test with (left) and without (right) residual stretches.	54
Figure 3.17: Circumferential strain of aortic segment with (left) and without (right) residual stretches.....	54
Figure 3.18: Axial strain of aortic segment with (left) and without (right) residual stretches.	54
Figure 3.19: Pressure - Axial stretch curves for varied axial pre-strains (from 0% to 20%) with and without consideration of residual stretches	55
Figure 3.20: Pressure - Circumferential stretch curves for varied axial pre-strains (from 0% to 20%) with and without consideration of residual stretches	55
Figure 3.21: Displacement in z-direction, impactor acceleration and energy of impact test.....	56
Figure 3.22: Deformation at different time steps for model A (left) and model B (right)	57
Figure 3.23: Result of pre-simulation - seat belt	58
Figure 3.24: Result of pre-simulation - aorta segments	58
Figure 3.25: Result of pre-simulation - heart.....	59
Figure 3.26: Simulation result with GHBMCO F05 at different time steps	60

7 List of tables

Table 1.1: AIS severity of thorax injuries (Schmitt et al., 2010)	7
Table 1.2: Frontal impact tolerances of the chest for viscous criteria (Nahum and Melvin, 2002)	13
Table 1.3: Frontal impact tolerance of the chest for the combined thorax index (Nahum and Melvin, 2002)	14
Table 1.4: Advantages and disadvantages of each criteria	14
Table 1.5: Comparison of different aortic models of HBM-occupants.....	15
Table 1.6: Overview of phenomenological models for arterial tissue	18
Table 2.1: Used AIS-Codes for accident analysis in CEDATU	28
Table 2.2: Structure of Matlab-source code for calculating the 'Freed-Einstein' model	30
Table 2.3: Short explanation of parameters used in Matlab for Freed-Einstein material of LS-Dyna.....	32
Table 2.4: Parameters, sensors and expressions used for inflation test with a short explanation	36
Table 3.1: Registered cases in CEDATU with TRA-injury	43
Table 3.2: TRA-killed persons, Comparison Statistik Austria - CEDATU	49
Table 3.3: Parameters for exponential model	50
Table 3.4: Results from HyperStudy parameter fitting	50

8 References

- Anderson, S.A., Day, M., Chen, M.K., Huber, T., Lottenberg, L.L., Kays, D.W., Beierle, E.A., 2008. Traumatic aortic injuries in the pediatric population. *J. Pediatr. Surg.* 43, 1077–1081. doi:10.1016/j.jpedsurg.2008.02.030
- Artner, T., 2016. Modellierung eines Aortensegments unter dynamischer Belastung. *Veh. Saf. Inst. Univ. Technol. Graz.*
- Benjamin, M.M., Roberts, W.C., 2012. Fatal aortic rupture from nonpenetrating chest trauma. *Proc. Bayl. Univ. Med. Cent.* 25, 121–123.
- Burkhart, H.M., Gomez, G.A., Jacobson, L.E., Pless, J.E., Broadie, T.A., 2001. Fatal blunt aortic injuries: A review of 242 autopsy cases. *J. Trauma* 50, 113–115.
- Chatterjee, K., Anderson, M., Heistad, D., Kerber, R.E., 2012. *Cardiology - An illustrated textbook.* Jaypee Brothers Medical Publisher, New Delhi.
- Cohen, A.M., Crass, J.R., Thomas, H.A., Fisher, R.G., Jacobs, D.G., 1992. CT evidence for the “osseous pinch” mechanism of traumatic aortic injury. *Am. J. Roentgenol.* 159, 271–274. doi:10.2214/ajr.159.2.1632338
- Crass, J.R., Cohen, A.M., Motta, A.O., Tomashefski, J.F., Wiesen, E.J., 1990. A proposed new mechanism of traumatic aortic rupture: the osseous pinch. *Radiology* 176, 645–649. doi:10.1148/radiology.176.3.2389022
- Delfino, A., Stergiopoulos, N., Moore, J.E., Meister, J.J., 1997. Residual strain effects on the stress field in a thick wall finite element model of the human carotid bifurcation. *J. Biomech.* 30, 777–786.
- Demetriades, D., 2012. Blunt Thoracic Aortic Injuries: Crossing the Rubicon. *J. Am. Coll. Surg.* 214, 247–259. doi:10.1016/j.jamcollsurg.2011.11.015
- Demetriades, D., Murray, J., Martin, M., Velmahos, G., Salim, A., Alo, K., Rhee, P., 2004. Pedestrians injured by automobiles: Relationship of age to injury type and severity 1. *J. Am. Coll. Surg.* 199, 382–387. doi:10.1016/j.jamcollsurg.2004.03.027
- Eichinger, W.B., von Canal, F., Lange, R., 2001. *Aortic Dissection. Up-date in Vascular Surgery.* Foxwell Davies Ltd Sci. Publ. Lond. 65–77.
- Eisenach, A., 2014. Entwicklung eines numerischen Menschmodells für ein drei Jahre altes Kind. doi:http://dx.doi.org/10.14279/depositonce-4037
- Escobar, M.A., Caty, M.G., 2011. Thoracic Injuries in Children, in: *Pediatric Critical Care.* Elsevier, pp. 1520–1527.
- Forman, J., Stacey, S., Evans, J., Kent, R., 2008. Posterior acceleration as a mechanism of blunt traumatic injury of the aorta. *J. Biomech.* 41, 1359–1364. doi:10.1016/j.jbiomech.2008.01.020

- Freed, A.D., Einstein, D.R., Vesely, I., 2005. Invariant formulation for dispersed transverse isotropy in aortic heart valves: An efficient means for modeling fiber splay. *ResearchGate* 4, 100–17. doi:10.1007/s10237-005-0069-8
- Fung, Y.C., Fronek, K., Patitucci, P., 1979. Pseudoelasticity of arteries and the choice of its mathematical expression. *Am. J. Physiol. - Heart Circ. Physiol.* 237, H620–H631.
- Gresik, C., Esposito, T., Hommel, D., Glynn, L., Love, R., 2013. Blunt thoracic aortic injury in pediatric patients. *Surg. Sci.* 4, 160–165. doi:http://dx.doi.org/10.4236/ss.2013.42031
- Hardy, W.N., Shah, C.S., 2006. Study of Potential Mechanisms of Traumatic Rupture of the Aorta Using InSitu Experiments. *Stapp Car Crash J. Vol 50 2006 - P-398* 20.
- Hardy, W.N., Shah, C.S., Mason, M.J., Kopacz, J.M., Yang, K.H., King, A.I., Bishop, J.L., Banglmaier, R.F., Bey, M.J., Morgan, R.M., Digges, K.H., 2008. Mechanisms of Traumatic Rupture of the Aorta and Associated Peri-isthmus Motion and Deformation. *Stapp Car Crash J. Vol. 52*, 233–265.
- Holzappel, G.A., Gasser, T.C., Ogden, R.W., 2000. A New Constitutive Framework for Arterial Wall Mechanics and a Comparative Study of Material Models. *J. Elast. Phys. Sci. Solids* 61, 1–48. doi:10.1023/A:1010835316564
- Holzappel, G.A., Ogden, R.W., 2003. *Biomechanics of Soft Tissue in Cardiovascular Systems*, International Centre for Mechanical Sciences, Courses and Lectures. Springer Vienna.
- Humphrey, J.D., 1999. An evaluation of pseudoelastic descriptors used in arterial mechanics. *J. Biomech. Eng.* 121, 259–262.
- Kodali, S., Jamieson, W.R., Leia-Stephens, M., Miyagishima, R.T., Janusz, M.T., Tyers, G.F., 1991. Traumatic rupture of the thoracic aorta. A 20-year review: 1969-1989. *Circulation* 84, 1140-46.
- Lee, S.-H., Kent, R., 2007. Blood flow and fluid-structure interactions in the human aorta during traumatic rupture conditions. *Stapp Car Crash J.* 51, 211–233.
- Lippert, H., 2010. Kapitel 4 - Leibeswand, Kapitel 10 - Herz, in: *Anatomie*. Urban & Fischer, München, pp. 84-85; 252-265.
- Lundevall, J., 1964. The mechanism of traumatic rupture of the aorta. *Acta Path Microbiol Scandinav* 62, 34–46.
- McGwin, G., Reiff, D.A., Moran, S.G., Rue, L.W., 2002. Incidence and characteristics of motor vehicle collision-related blunt thoracic aortic injury according to age. *J. Trauma* 52, 859–866.
- Moar, J.J., 1985. Traumatic rupture of the thoracic aorta. *Afr Med J* 67, 383–385.
- Nahum, A.M., Melvin, J., 2002. *Accidental Injury: Biomechanics and Prevention*. Springer Science & Business Media.
- Otte, D., Facius, T., Klintschar, M., Brand, S., 2016. Investigations and Injury Mechanisms of Aortic Ruptures among Vehicle Occupants and Vulnerable Road Users over Time. *IRCOBI Conf.* 870–887.
- Richens, D., Field, M., Neale, M., Oakley, C., 2002. The mechanism of injury in blunt traumatic rupture of the aorta. *Eur. J. Cardiothorac. Surg.* 21, 288–293.

- Richens, D., Kotidis, K., Neale, M., Oakley, C., Fails, A., 2003. Rupture of the aorta following road traffic accidents in the UK 1992-1999. *Eur. J. Cardiothorac. Surg.* 23, 143–148.
- Ryb, G.E., Dischinger, P.C., Kleinberger, M., McGwin, G., Griffin, R.L., 2013. Aortic injuries in newer vehicles. *Accid. Anal. Prev.* 59, 253–259. doi:10.1016/j.aap.2013.06.007
- Sadaghianloo, N., Jean-Baptiste, E., Breaud, J., Declémy, S., Kurzenne, J.-Y., Hassen-Khodja, R., 2014. Blunt abdominal aortic trauma in paediatric patients. *Injury* 45, 183–191. doi:10.1016/j.injury.2012.10.033
- Sartorelli, K.H., Vane, D.W., 2004. The diagnosis and management of children with blunt injury of the chest. *Semin. Pediatr. Surg.* 13, 98–105. doi:10.1053/j.sempedsurg.2004.01.005
- Schmitt, K.-U., Walz, F., Muser, M.H., Niederer, P.F., 2010. Thoraxverletzungen, in: *Trauma-Biomechanik. Verletzungen in Straßenverkehr und Sport*. Springer-Verlag, pp. 157–179.
- Schreiber, C., Pörner, M., Tassani-Prell, P., Kostolny, M., Eicken, A., Lange, R., 2006. Aortic Aneurysm 31 Years after Coarctation Repair with Direct Anastomosis. *Herz Kardiovaskuläre Erkrank.* 31, 75–77. doi:10.1007/s00059-006-2760-7
- Sevitt, S., 1977. The mechanisms of traumatic rupture of the thoracic aorta. *Br. J. Surg.* 64, 166–173. doi:10.1002/bjs.1800640305
- Shah, C.S., 2007. Investigation of traumatic rupture of the aorta (TRA) by obtaining aorta material and failure properties and simulating real-world aortic injury crashes using the whole-body finite element (FE) human model (Ph.D.). Wayne State University, United States -- Michigan.
- Shah, C.S., Yang, K.H., Hardy, W.N., Wang, K., King, A.I., 2001. Development of a computer model to predict aortic rupture due to impact loading. *Stapp Car Crash J.* 45, 161–182.
- Sommer, G., Holzapfel, G.A., 2012. 3D constitutive modeling of the biaxial mechanical response of intact and layer-dissected human carotid arteries. *J. Mech. Behav. Biomed. Mater.* 116–128.
- Steffan, H., Tomasch, E., 2006. CEDATU - A central database of fatalities in Austria. *Int. Conf. ESAR - Expert Symp. Accid. Res.*
- Takamizawa, K., Hayashi, K., 1987. Strain energy density function and uniform strain hypothesis for arterial mechanics. *J. Biomech.* 20, 7–17.
- Törő, K., Hubay, M., Sótonyi, P., Keller, E., 2005. Fatal traffic injuries among pedestrians, bicyclists and motor vehicle occupants. *Forensic Sci. Int.* 151, 151–156. doi:10.1016/j.forsciint.2005.01.014
- Tribble, C.G., Crosby, I.K., 1988. Traumatic Rupture of the Thoracic Aorta. *South. Med. J.* 963–968.
- Vaishnav, R.N., Young, J.T., Patel, D.J., 1973. Distribution of Stresses and of Strain-Energy Density through the Wall Thickness in a Canine Aortic Segment. *Circ. Res.* 32, 577–583. doi:10.1161/01.RES.32.5.577
- Voigt, G.E., Wilfert, K., 1969. Mechanisms of Injuries to Unrestrained Drivers in Head-On Collisions. *SAE Int.* 11. doi:10.4271/690811
- Weisbecker, H., Pierce, D.M., Regitnig, P., Holzapfel, G.A., 2012. Layer-specific damage experiments and modeling of human thoracic and abdominal aortas

- with non-atherosclerotic intimal thickening. *J. Mech. Behav. Biomed. Mater.* 12, 93–106. doi:10.1016/j.jmbbm.2012.03.012
- Weisbecker, H., Unterberger, M.J., Holzapfel, G.A., 2015. Constitutive modelling of arteries considering fibre recruitment and three-dimensional fibre distribution (PDF Download Available). *J. R. Soc. Interface.* doi:http://dx.doi.org/10.1098/rsif.2015.0111
- White, N.A., Shah, C.S., Hardy, W.N., 2010. Mechanisms of Traumatic Rupture of the Aorta: Recent Multi-scale Investigations, in: Herold, K.E., Vossoughi, J., Bentley, W.E. (Eds.), 26th Southern Biomedical Engineering Conference SBEC 2010, April 30 - May 2, 2010, College Park, Maryland, USA, IFMBE Proceedings. Springer Berlin Heidelberg, pp. 452–455. doi:10.1007/978-3-642-14998-6_115
- Yokoyama, H., Ohmi, M., Sadahiro, M., Shoji, Y., Tabayashi, K., Moizumi, Y., 2000. Spontaneous Rupture of the Thoracic Aorta. *Soc. Thorac. Surg.* 70, 683–689.
- Zehnder, M.A., 1960. Unfallmechanismus und Unfallmechanik der Aortenruptur im geschlossenen Thoraxtrauma. *Thoraxchirurgie* 8, 47–65. doi:10.1055/s-0028-1101280

Deutsches Herz Zentrum München (2015)

http://www.dhm.mhn.de/de/kliniken_und_institute/klinik_fuer_herz-_und_gefaessc/chirurgie_bei_erworbenen_herzf/fachwissen/gefaesserkrankungen/traumatische_aortenruptur.cfm (access 2016-01-25)

Gumpert (2015)

http://www.dr-gumpert.de/html/gefaessversorgung_herz.html (access 2015-07-23)

HyperStudy, Altair HyperWorks (2016)

<http://www.altairhyperworks.com/product/hyperstudy> (access 2017-02-11)

NHTSA (2015)

<http://www.nhtsa.gov/Research/Vehicle+Research+&+Testing+%28VRTC%29/Hybrid+III+5th+Percentile+Female> (access 2015-12-18)

Rakesh Sharmahi (2014)

<https://www.slideshare.net/rakeshsharmahitech/aortic-dissection-01> (access 2017-05-05)

StatCube – Statistik Austria (2015)

<http://statcube.at/statistik.at/ext/statcube/jsf/terms.xhtml> (access 2015-11-14)

Statistik Austria (2015)

http://www.statistik.at/web_de/statistiken/energie_umwelt_innovation_mobilitaet/verkehr/strasse/unfaelle_mit_personenschaden/019874.html (access 2015-10-21)

U.S. National Library of Medicine (2017)

<https://ghr.nlm.nih.gov/gallery> (access 2017-05-05)

Wayne State University – CHARM (2016)

<https://automotivesafety.wayne.edu/charm-10> (access 2016-02-20)